CHAPTER 2.

CHAPTER 2.

Literature Review and Background Theory

The purpose of this Chapter is to summarise previous work on flow and dispersion in complex terrain and, where appropriate, to develop some of the theory. A brief introduction is necessary to permit the reader to navigate the various strands.

This review is subdivided into three main topics: experimental measurements, analytical theory and numerical computation. The equally important subjects of turbulence modelling and the structure and simulation of the atmospheric boundary layer are treated in Chapters 4 and 5 respectively, where further literature related to these will be reviewed.

In Section 2.1 the selection of experimental measurements is divided into field and laboratory studies. In Section 2.2 we review various analytical models for neutral and stably stratified flow and dispersion over surface topography. The first three are essentially inviscid: linear, finite-amplitude and low-Froude-number theories. The fourth considers turbulent shear flow over low hills of the form typified by Jackson-Hunt theory. The last subsection summarises existing dispersion models for routine and regulatory use. Finally, in Section 2.3 we consider numerical modelling of flow and dispersion in complex terrain.

2.1 Experimental Measurements of Flow and Dispersion in Complex Terrain

Although a qualitative description of airflow in complex terrain had been extant for some time, Jackson and Hunt (1975) provided the first satisfactory theory matching the outer-layer disturbance caused by streamline displacement over undulating terrain with the turbulent shear layer near the ground. Although the model has since been refined and extended, the central premise still stands - a division of the flow into an *outer* layer, where the flow perturbation is essentially inviscid (driven by pressure fields generated by streamline displacement), and an *inner* layer, where the turbulent shear stress is important and is described by a mixing-

length model. We shall examine this theory in greater detail later.

In their challenging 1975 paper, Jackson and Hunt not only established a firm foundation for future theoretical development, but emphasised the need for experimentalists to provide them with data with which to validate their model. Since then, a large number of experimental studies - both in the field and in the laboratory - have been instigated. An excellent review of the full-scale measurements has been given by Taylor et al. (1987).

2.1.1 Field Studies

Perhaps the first full-scale experimental study specifically designed to test the predictions of Jackson-Hunt theory was that of Mason and Sykes (1979a) at Brent Knoll in Somerset. In the same paper the authors presented the natural extension of the original two-dimensional theory to three dimensions, so opening up the practical application of the model to real terrain. Measurement detail was comparatively limited, being restricted to mean wind speed measurements at 2m above the surface. Nevertheless, it did allow an assessment of the global predictions of the model - such as the maximum speed-up at the summit - to be made. The British Meteorological Office followed this up with more detailed measurement programmes at other isolated hills: the island of Ailsa Craig (Jenkins et al., 1981), Blashaval (Mason and King, 1985) and Nyland Hill (Mason, 1986).

Meanwhile, on the other side of the world, CSIRO were making use of a redundant television mast to make measurements of mean and turbulent wind profiles over the summit of Black Mountain, near Canberra (Bradley, 1980). A local velocity maximum or "jet" was observed at a height and of a magnitude consistent with Jackson-Hunt theory, despite the manifest violation of the low-slope, two-dimensional assumptions of that model. The influence of (weak) thermal stability and non-normal wind incidence angles were investigated in a follow-up study at Bungendore Ridge (Bradley, 1983). Observations showed that the maximum speed-up factor, $\Delta S \equiv (U(z)-U_a(z))/U_a(z)$, varied in a manner consistent with changes to the approach-flow mean wind speed profile occasioned by stability. According to Jackson-Hunt theory,

$$\Delta S_{max} = \frac{\Delta U(\ell)}{U(\ell)} \sim \sigma \frac{H}{L}\left(\frac{U(L)}{U(\ell)}\right)^2 \tag{2.1}$$

where H is the height of the hill, L the *half-length* (average radius from the summit of the ½H contour), ℓ is the inner-layer height (see later) and σ is a shape factor of order unity. The approach-flow mean wind speed may (at least in the surface layer) be described by Monin-Obukhov similarity theory (Chapter 5):

$$U(z) = \frac{u_*}{\kappa}[\ln(z/z_0) + 5z/L_{MO}] \tag{2.2}$$

giving a characteristic variation in the maximum speed-up as the Monin-Obukhov length varies. The study also flagged the importance of a roughness transition over the hill, a feature to which we will return later. More recently, the same organisation has made a more detailed series of measurements examining the effects of thermal stability at Coopers Ridge (Coppin et al., 1994).

Probably the most detailed of all wind-field measurement programs was undertaken at Askervein, a 116m-high hill on South Uist in the Outer Hebrides, as part of an International Energy Agency program on research and development into wind energy. Spatial resolution was obtained from several linear arrays of anemometers at 10m from the ground, supplemented by profile data from fixed masts up to 50m in height at key locations, including the summit and a reference site upwind. Further TALA kite and airsonde releases provided some wind measurements at greater heights. An overview of the experiment can be found in Taylor and Teunissen (1987), analysis of the spatial variation of wind speed in Salmon et al. (1988) and profile data in Mickle et al. (1988). This was a remarkable project because the program also included wind-tunnel simulations at three scales (Teunissen et al., 1987) and a finite-volume calculation (Raithby et al., 1987).

A number of full-scale measurements of atmospheric dispersion have also been carried out in regions of complex terrain. These include both monitoring studies for existing industrial pollution sources - such as power stations and incinerators - and deliberate releases near isolated terrain features to study generic effects. Even in the former case it is common to

inject and track an artificial tracer, since this eliminates errors due to natural background and uncertainty in the source strength. The tracers used must be stable, non-toxic and detectable at low concentrations. Sulphur hexafluoride (SF_6) and the halocarbons C_2Cl_4 and CH_3Br have been widely used. Most quantitative studies have focused on ground-level concentrations, although advances in remote sensing technology - in particular, the development of LIDAR (**L**aser **I**nterferometry **D**etection **A**nd **R**anging) - now permit the resolution of vertical plume structure. The mobility of vehicle-mounted instrumentation also has benefits over fixed sampling arrays when the ambient wind direction is unreliable.

Maryon et al. (1986) followed up the earlier flow measurements by Mason and King (1985) at Blashaval with a point-source diffusion study in neutral conditions. A limited sampling array on the upwind slope was able to measure crosswind spread and vertical plume profiles up to 15m (for a source height of 8m). Concentration measurements were consistent with flow divergence in the horizontal and convergence in the vertical, bringing the plume closer to the ground. Building on experience gained from this study, the UK Meteorological Office carried out a second dispersion study in neutrally stable conditions at Nyland Hill (Mylne and Callander, 1989). In this experiment dual tracers were emitted simultaneously from two heights. Plume crosswind spread confirmed the effects of flow divergence and was greater for the lower source.

The effect of horizontal divergence is greater in stably stratified flows, where vertical deflection of streamlines is suppressed by buoyancy forces. A number of well-documented studies have been carried out in the United States to characterise dispersion from upwind sources in strongly stable flow. These include the EPA Complex Terrain Model Development Program experiments at Cinder Cone Butte and Hogback Ridge (Strimaitis et al., 1983). The first of these will be discussed in more detail in Chapter 6, where the results of a numerical comparison are presented. Dispersion studies were also conducted by Ryan et al. (1984) at the much higher Steptoe Butte (340m). In this experiment tracer gases were released (from a tethered balloon support) at heights up to 190m. These measurements demonstrated considerable sensitivity to wind direction in flows for which $Fr<1$ (where $Fr=U/NH$ is the Froude number based on hill height), with strong lateral divergence and, in many cases, plume impaction on the surface. They also confirmed the usefulness of the "dividing-streamline

height", a representative height determined from the approach-flow velocity and density profiles which, on energy grounds, distinguishes fluid with sufficient kinetic energy to surmount the hill from that which must pass around the sides. We shall consider this concept in more detail below.

2.1.2 Laboratory Simulation

Laboratory simulation of environmental flow and dispersion is seen as an attractive alternative to full-scale field experiments, particularly where a large matrix of inflow conditions and/or source configurations are to be investigated. The commonest types of facility are wind tunnels and water channels/towing tanks, with rotating tanks to investigate larger scale phenomena where the effect of the earth's rotation becomes important. For atmospheric flows, recognition of the importance of buoyancy forces has led to the development of facilities for simulating density changes in the flow - thermally stratified wind tunnels and salinity-stratified towing tanks. The similarity criteria which must be met in such scale simulations have been reviewed by Snyder (1972) and Baines and Manins (1989).

The development of a quasi-equilibrium, deep turbulent boundary layer within a short fetch is something of an art in itself. A common configuration uses a combination of low-level trip and upright tapered elements at inflow, together with an artificially roughened floor (Robins, 1977). The wind-tunnel roof imposes a blockage effect which is not to be found in the unbounded atmosphere. There is an outstanding controversy as to whether a zero-pressure-gradient condition (obtained by locally raising or lowering the wind-tunnel roof) is the appropriate means of eliminating this effect over two-dimensional topography.

Two effects complicating interpretation of results and the maintenance of steady conditions in a towing tank which are not present in the real atmosphere are described by Snyder et al. (1985). The first is the "squashing" or "blocking" phenomenon, whereby incompressible fluid is obliged to pile up ahead of an obstacle by the finite length of the tank, returning over the top to alter permanently the upstream density profile. The second results from the finite depth of the tank supporting upstream-propagating columnar modes, which may, in their turn, reflect

from the upstream boundary. In the atmosphere, upward-propagating gravity waves radiate to infinity, whereas, in a towing tank, they are reflected from floor or free surface. Baines and Hoinka (1985) describe a novel means of overcoming this in the laboratory by partitioning their towing tank lengthways and deflecting outgoing waves out of the working side by means of an angled plate.

A number of investigations have been carried out specifically to correlate the results of laboratory and full-scale experiments. These include detailed comparisons for Gebbies Pass (Neal, 1983) and the Askervein project (Teunissen et al., 1987). In the latter case, wind-tunnel experiments were carried out at three scales. Snyder and Lawson (1981) describe towing-tank simulations of the Cinder Cone Butte dispersion study. Wind-tunnel simulations of complex terrain have been used extensively in planning studies for large industrial plant. To date, the majority of wind-tunnel simulations of real terrain have been conducted in neutral stability. A recent exception is the simulation of stably stratified flow around Mt Tsukuba in Japan (Kitabayashi, 1991) using distorted vertical scaling.

Whilst detailed topographic models are undoubtably necessary for site-specific studies, they are time-consuming and expensive to manufacture and do not readily lend themselves to a fundamental understanding of the flow. For these reasons the majority of wind-tunnel simulations have concentrated on simpler generic shapes. Bowen and Lindley (1977) examined the speed-up over escarpments of various shapes, whilst Pearse et al. (1981) and Arya and Shipman (1981) measured deep boundary-layer flow over two-dimensional ridges. Arya et al. (1981) followed this up with measurements of diffusion from a point source in the same flow. Castro and Snyder (1982) measured concentrations from sources downwind of finite-length ridges and a cone. Their experiments were extended to non-normal wind incidence by Castro et al. (1988). For dispersion around three-dimensional conical hills, Arya and Gadiyaram (1986) and Snyder and Britter (1987) reported measurements of dispersion from downwind and upwind sources respectively.

Among the general conclusions to be drawn from these studies about topography-affected dispersion in neutral conditions are that, for *upwind* sources, the terrain amplification factor (ie, the relative increase in maximum ground-level concentration over the flat-terrain case)

is likely to be less for two-dimensional than three-dimensional topography, since, in the former case, the streamlines pass further from the hill. For *downwind* sources, the reverse is true, since two-dimensional flows exhibit stronger downwash - with or without flow separation. The effect of this downwash - caused by a net downflow of fluid as the velocity recovers in the wake - may lead to significant terrain amplification factors. Castro and Snyder (1982) report values of 1.5 - 3.0 even for sources downwind of the separated-flow reattachment point.

Of greater practical significance for real terrain are flow and dispersion measurements over curved hills. (These represent a greater challenge in turbulence modelling and numerical simulation since, unlike bluff body shapes, neither the onset nor the location of flow separation is determinable from the geometry.) Britter et al. (1981) studied slope and roughness effects over two-dimensional bell-shaped hills, whilst Khurshudyan et al. (1981) and Snyder et al. (1991) made detailed flow and dispersion measurements around isolated two-dimensional hills ("RUSHIL" experiment) and the inverted valley configuration ("RUSVAL" experiment). Data from the RUSHIL experiment will be simulated using the SWIFT code in Chapter 6. Gong and Ibbetson (1989) and Gong (1991) reported flow and dispersion measurements over two- and three-dimensional hills of cosine-squared cross-section.

Towing-tank experiments on stably stratified flow around axisymmetric hills were conducted by Hunt and Snyder (1980). These investigated the range of application of Drazin's (1961) low-Froude-number theory and how the lee-wave structure affected separation behind the hill. In the latter aspect, they found that separation was boundary-layer controlled when the lee wavelength $2\pi U/N$ was much longer than the length of the hill, but was totally suppressed when the two were of the same order. As Froude numbers were reduced even further, separation under a downstream rotor was provoked by the lee-wave field.

2.2 Theoretical Models

2.2.1 Linear Theory

Few would argue that the least tractable feature of the Navier-Stokes equations is their inherent non-linearity. Since exact analytical solutions are seldom available, it is a common, and not unreasonable, practice to see how far one can get by linearising the equations of motion.

The small-perturbation analysis was developed for wave motions and the classical instability problem by such "giants" of the last century as Stokes (1847), Lord Kelvin (W.Thompson) (1879) and Lord Rayleigh (1880). At the turn of the century, Ekman (1904) was explaining the increased drag on ships by means of internal gravity waves developed on the interface between fresh and saline water in coastal regions. (A nice photograph of his laboratory simulation can be found in Gill, 1982, p124.) The analysis of discrete layers was extended to the continuously stratified case by, amongst others, Lord Rayleigh (1883), although it was papers by Brunt (1927) and his Norwegian counterpart Väisälä which brought to meteorology what had already been well developed by the naval architects.

Important solutions for linear internal waves forced by topography in an unbounded atmosphere were obtained by Lyra (1943) and Queney (1948), whilst Scorer (1949) extended the uniform-velocity results to include the effects of upstream velocity shear. We shall examine his equation in more detail below. One of the most important principles of linearised theory is that of superposition, enabling the perturbation for arbitrarily shaped topography to be generated from the integral sum of individual Fourier modes. Whilst straightforward to derive analytically (Crapper, 1959), the general picture of disturbances arising from three-dimensional topography is considerably more complex than its two-dimensional counterpart. The lee-wave structure has been examined by Sawyer (1962). Smith (1980) presents an excellent picture of the three-dimensional flow fields forced by topography and discusses the effect of the hydrostatic assumption on near-surface and far-field perturbations to the flow. The linear analysis is reworked in isosteric coordinates in Smith (1988). Although the hydrostatic approximation is widely used as a simplifying assumption, its validity for typical

atmospheric profiles is often questionable (Keller, 1994).

Whilst many analytical results have been obtained for specific stability profiles (and the uniform-velocity, constant-density-gradient situation is about the most commonly analysed and least realistic of them), actual velocity and temperature profiles may exhibit considerable variation. One of the most useful tools for analysing disturbances in non-uniform stratification is *ray-tracing* (Lighthill, 1978).

Having given due credit to historical precedence we shall now examine mathematically some of the results of linearised theory.

For small-amplitude disturbances to a Boussinesq, inviscid fluid with plane-parallel velocity profile $\vec{U}(z)=(U(z),0,0)$ and density profile $\rho_a(z)$, the continuity and momentum equations and the incompressibility condition are, respectively,

$$\nabla\bullet\vec{u} = 0 \tag{2.3}$$

$$\rho_0\left(\frac{D\vec{u}}{Dt} + w\frac{d\vec{U}}{dz}\right) = -\nabla p + \rho\vec{g} \tag{2.4}$$

$$\frac{D\rho}{Dt} + w\frac{d\rho_a}{dz} = 0 \tag{2.5}$$

where $\vec{u}$, p and ρ are the perturbation velocity, pressure and density fields and $\frac{D}{Dt}\equiv\frac{\partial}{\partial t}+\vec{U}\bullet\nabla$ is the material derivative following the undisturbed flow.

Applying the operator $\nabla\wedge(\nabla\wedge\ )\equiv\nabla(\nabla\bullet\ )-\nabla^2$ to the momentum equation and taking the resulting vertical component gives

$$\frac{D}{Dt}\nabla^2 w - \frac{d^2U}{dz^2}\frac{\partial w}{\partial x} = -\frac{g}{\rho_0}\nabla_h^2\rho \tag{2.6}$$

which, on using the incompressibility equation to eliminate ρ, leads to an equation for the vertical velocity component w:

$$\frac{D}{Dt}\left(\frac{D}{Dt}\nabla^2 w - \frac{d^2U}{dz^2}\frac{\partial w}{\partial x}\right) + N^2\nabla_h^2 w = 0 \tag{2.7}$$

where $N \equiv \left(-\frac{g}{\rho_0}\frac{d\rho_a}{dz}\right)^{1/2}$ is the *buoyancy* or *Brunt-Väisälä frequency*. Since this equation is homogeneous and linear, with coefficients which are functions of z only, it can be Fourier-transformed in horizontal coordinates and time. Considering a single harmonic component $\tilde{w}(z;k,l,\omega)e^{i(kx+ly-\omega t)}$, equation (2.7) is equivalent to the following equation in Fourier space:

$$\frac{\partial^2\tilde{w}}{\partial z^2} - \frac{1}{U-c}\frac{d^2U}{dz^2}\tilde{w} + \left[\frac{N^2}{(U-c)^2} - k^2\right]\left(\frac{k^2+l^2}{k^2}\right)\tilde{w} = 0 \tag{2.8}$$

where $c \equiv \omega/k$ is the along-wind phase velocity.

The primary applications of equations (2.7) or (2.8) are to

- hydrodynamic stability;
- internal waves forced by topography.

We shall examine each of these in turn.

Firstly, the hydrodynamic stability problem. For the harmonic component $\tilde{w}(z)e^{i[k(x-ct)+ly]}$ (with the implicit dependence of $\tilde{w}$ on wavenumber and frequency dropped for clarity), a growing disturbance or instability is distinguished by $c_i \equiv \mathrm{Im}(c)>0$.

N is the frequency of small-amplitude oscillations of a particle displaced vertically in a stratified fluid. The relative strength of buoyancy and shear may be expressed by the *gradient Richardson number Ri*, the (squared) ratio of shear to buoyancy timescales:

$$Ri = \frac{N^2}{\left|\frac{d\vec{U}}{dz}\right|^2} \tag{2.9}$$

According to a result conjectured by G.I. Taylor and first proved by Miles (1961), a *necessary* condition for instability (a precursor to turbulence) for a plane-parallel shear flow is that $Ri<¼$ somewhere in the flow. This paper in the Journal of Fluid Mechanics was followed by an alternative proof by Howard (1961), which is so appealingly neat that it is worthwhile

repeating (in the current notation and extended to three dimensions) here. Making the substitution $H=\dfrac{\tilde{w}}{(U-c)^n}$ in (2.8), one obtains

$$\frac{\partial}{\partial z}\left[(U-c)^{2n}\frac{\partial H}{\partial z}\right] + \left\{(U-c)^{2n-2}\left[n(n-1)\left(\frac{dU}{dz}\right)^2+N^2\left(\frac{k^2+l^2}{k^2}\right)\right]+(U-c)^{2n-1}\left[(n-1)\frac{d^2U}{dz^2}\right]-(U-c)^{2n}(k^2+l^2)\right\}H = 0 \tag{2.10}$$

Multiplying by the complex conjugate $\overline{H}$ and integrating, this can be rearranged to give

$$\begin{aligned}&\int_{z_1}^{z_2}(U-c)^{2n}\left[\left|\frac{\partial H}{\partial z}\right|^2+(k^2+l^2)\,|H|^2\right]dz\\ &+\int_{z_1}^{z_2}(U-c)^{2n-1}(1-n)\frac{d^2U}{dz^2}\,|H|^2dz\\ &+\int_{z_1}^{z_2}(U-c)^{2n-2}\left[n(1-n)\left(\frac{dU}{dz}\right)^2-N^2\left(\frac{k^2+l^2}{k^2}\right)\right]|H|^2dz = 0\end{aligned} \tag{2.11}$$

(The first term has been integrated by parts, assuming w to vanish on z_1 and z_2, which may be at $\pm\infty$.)

Choosing n=½, and taking imaginary parts, we obtain

$$-c_i\int_{z_1}^{z_2}\left\{\left|\frac{\partial H}{\partial z}\right|^2 + (k^2+l^2)\,|H|^2 + \left[N^2\left(\frac{k^2+l^2}{k^2}\right)-\frac{1}{4}\left(\frac{dU}{dz}\right)^2\right]\frac{|H|^2}{|U-c|^2}\right\}dz = 0 \tag{2.12}$$

Hence, if $Ri\equiv\dfrac{N^2}{(dU/dz)^2}>\dfrac{1}{4}$ everywhere then c_i must be zero; ie, there is no instability. QED

As a side benefit, if we choose n=0 instead then we can derive another important result in hydrodynamic stability. Imaginary parts give

$$c_i\int_{z_1}^{z_2}\left(\frac{d^2U}{dz^2} - 2N^2\left(\frac{k^2+l^2}{k^2}\right)\frac{U-c_r}{|U-c|^2}\right)\frac{|H|^2}{|U-c|^2}dz = 0 \tag{2.13}$$

and hence a *necessary* condition for instability (non-zero c_i) is that

$$\frac{d^2U}{dz^2} - 2N^2\left(\frac{k^2+l^2}{k^2}\right)\frac{U-c_r}{|U-c|^2} \tag{2.14}$$

changes sign somewhere. This is a (rather unhelpful) extension to the stable case of Lord Rayleigh's uniform-density result that a necessary condition for instability is that the mean-velocity profile shall have an inflexion point: $d^2U/dz^2=0$.

The more important application for our present purposes is that of deriving the flow perturbation forced by isolated topography. In this case the forcing is derived from the lower boundary condition that the hill surface be a streamline: $(\vec{U}+\vec{u}).\nabla[z-Hf(x,y)]=0$. On the assumption that the hill height H is much less than a typical horizontal length scale, this linearises to

$$w = UH\frac{\partial f}{\partial x} \qquad \text{on } z=0 \tag{2.15}$$

or, in Fourier space,

$$\tilde{w}(0) = ikUH\tilde{f} \tag{2.16}$$

Referring to equation (2.8), we see that, in two dimensions, an approach flow with mean-velocity shear can be treated formally in the same way as unsheared flow, with $\left(\frac{N}{U-c}\right)^2$ replaced by $S^2(z)=\left(\frac{N}{U-c}\right)^2-\frac{1}{U-c}\frac{d^2U}{dz^2}$. However, no such wavenumber-independent simplification is possible in three dimensions, where $(k^2+l^2)/k^2\neq 1$. To make the problem tractable in three dimensions, then, we shall confine the analysis to the unsheared case, $U=constant$.

To emphasise the wave nature of the solution, equation (2.8) can be written

$$\frac{\partial^2\tilde{w}}{\partial z^2} + m^2\tilde{w} = 0 \tag{2.17}$$

where

$$m^2 = \left[\frac{N^2}{(kU-\omega)^2} - 1\right](k^2+l^2) \tag{2.18}$$

For uniform N, equation (2.17) admits wavelike solutions $\tilde{w}=\{e^{imz},e^{-imz}\}$ if $m^2>0$ and exponential solutions $\tilde{w}=\{e^{|m|z},e^{-|m|z}\}$ if $m^2<0$. (In this context, {,} means "a linear combination of".) For the wavelike solutions one has a dispersion relation (inverting (2.18)):

$$\omega = kU \mp N\sqrt{\frac{k^2+l^2}{k^2+l^2+m^2}} \tag{2.19}$$

with *group velocity*

$$\begin{aligned} \vec{c}_g &\equiv \nabla_k \omega \\ &= \vec{U} - (U-c)\left(\frac{k^2m^2}{(k^2+l^2)(k^2+l^2+m^2)}\ ,\ \frac{klm^2}{(k^2+l^2)(k^2+l^2+m^2)}\ ,\ \frac{-km}{k^2+l^2+m^2}\right) \end{aligned} \tag{2.20}$$

Again, $c=\omega/k$ is the along-wind *phase velocity*. The group-velocity vector $\vec{c}_g$ determines the rate and direction of wave-energy transport. (See Lighthill, 1978, for an excellent justification of this interpretation.)

In a *uniform*, *unbounded* atmosphere a steady-state (c=0) solution of (2.17) satisfying the lower boundary condition exists, with

$$\tilde{w} = \tilde{w}_0 e^{imz}\ , \qquad \tilde{w}_0 = ikUH\tilde{f} \tag{2.21}$$

where

$$m = \begin{cases} i(k^2+l^2)^{1/2}\sqrt{1-\left(\frac{N}{kU}\right)^2} & |k|>\frac{N}{U} \\ sgn(k)(k^2+l^2)^{1/2}\sqrt{\left(\frac{N}{kU}\right)^2-1} & |k|<\frac{N}{U} \end{cases} \tag{2.22}$$

For large wavenumbers (short wavelengths) the solution is that which decays (exponentially) with height. For small wavenumbers (long wavelengths) the wavelike solution is that for

which the radiation condition ($c_{gz} \equiv d\omega/dm > 0$) holds; ie, only *outgoing* wave energy is permitted. From (2.20) this requirement amounts to $mk>0$, fixing the sign of m. The wavelength $2\pi U/N$ which distinguishes the two cases is that of a fluid particle undertaking oscillations of frequency $N/2\pi$ whilst travelling at downwind speed U.

To consolidate we require expressions for the other flow variables. From the linearised equations (2.3) - (2.5), assuming a stationary solution with spatial dependence $e^{i(kx+ly+mz)}$, we have, from the horizontal momentum equation,

$$\begin{aligned} \tilde{u} &= -\frac{\tilde{p}}{\rho_0 U} \\ \tilde{v} &= -\frac{l}{k}\frac{\tilde{p}}{\rho_0 U} \end{aligned} \tag{2.23}$$

which, combined with the continuity equation, give

$$\tilde{w} = \frac{k^2+l^2}{km}\frac{\tilde{p}}{\rho_0 U} \tag{2.24}$$

These suffice to show how the horizontal wind is driven by the pressure field, which is itself derived from an interaction between the forced displacement of streamlines and ambient stratification. The incompressibility condition $\frac{D\rho}{Dt} + w\frac{d\rho_a}{dz} = 0$ yields

$$\tilde{\rho} g = \frac{\rho_0 N^2}{ikU}\tilde{w} \tag{2.25}$$

which, on substituting in the vertical momentum equation and transferring to the LHS, gives

$$\rho_0(\underline{ikU} + \frac{N^2}{ikU})\tilde{w} = -im\tilde{p} \tag{2.26}$$

The term underlined in (2.26) is that neglected in the *hydrostatic approximation* - that is, neglecting the advection term in the vertical momentum equation and determining the pressure by vertical integration of the buoyancy perturbation. From (2.26), we see that this corresponds to the long-wave limit $|k| \ll N/U$. In general, it will require that the typical horizontal scale

L of the topography be much longer than the wavelength associated with one buoyancy oscillation $2\pi U/N$. Dividing (2.26) by (2.24) we obtain the expression for the vertical wavenumber m as before:

$$m^2 = \left(\frac{N^2}{k^2U^2} - \underline{1}\right)(k^2+l^2) \tag{2.27}$$

In the hydrostatic approximation the underlined term vanishes and m^2 is always greater than 0 - ie, all Fourier modes are wavelike. Moreover, for two-dimensional disturbances (l=0) then $m=\pm N/U$, independent of horizontal wavenumber, so that two-dimensional hydrostatic waves are non-dispersive in the vertical.

Finally, we employ the linearised boundary condition (2.16) and invert (2.24) to obtain the pressure perturbation:

$$\tilde{p} = \tilde{p}_0 e^{imz} \tag{2.28}$$

where

$$\tilde{p}_0 = i\frac{k^2m}{k^2+l^2}\rho_0 U^2 H\tilde{f} \tag{2.29}$$

Equations (2.23), (2.24), (2.28) and (2.29), together with the vertical wavenumber (2.22), constitute the formal analytical expression for the perturbation induced by topography in a uniform, unbounded atmosphere. They are not particularly helpful for actually visualising the perturbation field and for this one must turn to flow patterns computed for specific topographic shapes. Smith (1980) considers the flow perturbations induced by an axisymmetric, bell-shaped hill with a particularly simple Fourier transform, describing the near-surface perturbation and far field, together with some discussion of the implications of the hydrostatic approximation. The asymptotic nature of the lee-wave field is also described in a highly mathematical paper by Janowitz (1984).

A number of general features of internal waves forced by topography are, however, indicated

by the analysis above.

- *Lee waves*. From the group-velocity expression (2.20) we have that $c_{gx}>0$: ie, for an unbounded atmosphere all wave energy is swept downstream and waves only appear in the lee of an obstacle. (This is in contrast to the bounded domain case, where disturbances can propagate upstream: see below.)
- *Constant phase lines slope backwards*. The radiation condition imposes $mk>0$: ie, m and k have the same sign. Thus, for constant y, the lines of constant phase, given by $kx+mz=constant$, have negative slope.
- *Group velocity and phase velocity are orthogonal*. Small-amplitude internal gravity waves constitute a *dispersive* system (phase velocity dependent on wavenumber) and wave energy propagates with the group velocity $\vec{c}_g$ rather than the phase velocity $\vec{c}_p$. For Fourier modes $w \propto e^{i(\vec{k}\bullet\vec{x}-\omega t)}$, equations (2.19) and (2.20) show that the phase velocity and group velocity are at right angles ($\vec{k}\bullet\vec{c}_g=0$) in a frame moving with the mean wind (U=0). (Actually, this is always true if the frequency depends on the direction but not the magnitude of the wavenumber vector $\vec{k}$). Equation (2.20) shows that phase and group velocities have:

  horizontal components of the same sign;

  vertical components of opposite signs.

  For stationary lee waves, we require $\vec{c}_p$ directed upwind (against the mean flow), whilst, for outgoing wave energy, we require $\vec{c}_g$ to have a positive vertical component. We have, therefore, the situation shown in Figure 2.1.
- *Gravity wave drag*. From equations (2.23) and (2.24), velocity and pressure perturbations are in phase (the constants relating $\tilde{u}_i$ to $\tilde{p}$ are real) and hence $<\vec{u}p>$ is non-zero. Thus, internal gravity waves are capable of transporting energy away from the point of production and, thereby, constitute a drag on topography. This has consequences in, for example, global climate models.

The Upper Boundary Condition

Hitherto we have analysed the case of a uniformly stratified, unbounded atmosphere. In this case the correct Fourier-mode solution is that which either decays or represents outward-

radiating energy. There are good theoretical and practical reasons for studying cases where wave energy is reflected, either by a rigid lid (or strong inversion) or a weakening density gradient which can no longer support internal waves.

We shall contrast the behaviour under two types of density profile:

- uniform stratification: $N=constant$;
- weakening stratification: $N=N_0 e^{-z/h}$.

In each case we shall consider two upper boundary conditions:

- unbounded atmosphere - for which the decaying or outgoing wave solution holds;
- rigid lid: $w=0$ on $z=D$.

Firstly, uniform stratification. Equation (2.17) admits solutions $\tilde{w}=\{e^{imz}, e^{-imz}\}$. Applying the boundary condition appropriate to finite or unbounded domains we have:

for an unbounded domain:

$$\tilde{w} = \begin{cases} \tilde{w}_0 e^{imz} & |k|<\dfrac{N}{U} \\ \tilde{w}_0 e^{-|m|z} & |k|>\dfrac{N}{U} \end{cases} \tag{2.30}$$

for a rigid lid at $z=D$:

$$\tilde{w} = \begin{cases} \tilde{w}_0 \dfrac{\sin m(D-z)}{\sin md} & |k|<\dfrac{N}{U} \\ \tilde{w}_0 \dfrac{\sinh |m|(D-z)}{\sinh |m|D} & |k|>\dfrac{N}{U} \end{cases} \tag{2.31}$$

In the first case the sign of m in the wavelike solution is chosen to satisfy the radiation condition $\partial\omega/\partial m>0$, which, from (2.20), implies $mk>0$ or $\mathrm{sgn}(m)=\mathrm{sgn}(k)$.

In the case of a rigid upper boundary, resonance can occur when the forcing is at one of the normal modes of the channel: $\sin|m|D=0$ or $mD=n\pi$, where n is an integer. Rearranging (2.19), this is possible for $\omega=0$ if

$$K^2 \equiv \left(\frac{ND}{\pi U}\right)^2 = n^2\left(\frac{k^2}{k^2+l^2}\right) + \frac{k^2D^2}{\pi^2} \tag{2.32}$$

In two dimensions (l=0) this can only occur for K>1. In three dimensions it is possible for all values of K.

For large wavenumbers ($|k|>N/U$) the rigid-lid solution (2.31) can be written

$$\tilde{w} = \tilde{w}_0\left(\cosh|m|z - \frac{\cosh|m|D}{\sinh|m|D}\sinh|m|z\right) \tag{2.33}$$

Since $\cosh|m|D/\sinh|m|D \to 1$ as $|m|D \to \infty$ and $\cosh|m|z - \sinh|m|z = e^{-|m|z}$ the short-wavelength solution for a finite domain tends to that for an unbounded domain as $D \to \infty$. However, for wavelike disturbances ($|k|<N/U$), then, except for very small $|m|z$ where the solution is essentially fixed by the boundary condition, the (linearised, inviscid) solution for a confined domain bears no resemblance to that for an infinite domain *for any value of D* and *all wave energy is reflected at the lid*.

By contrast, in *weakening* stratification, with $N=N_0e^{-z/h}$, wave motions can only propagate to some finite (wavenumber-dependent) height. If this lies well below the rigid lid then the effect of that restriction should be minimal. To analyse this we make the substitution

$$\zeta = \frac{N_0h}{|kU-\omega|}(k^2+l^2)^{1/2}e^{-z/h} \tag{2.34}$$

whence equation (2.17) becomes

$$\zeta^2\frac{d^2\tilde{w}}{d\zeta^2} + \zeta\frac{d\tilde{w}}{d\zeta} + (\zeta^2-\nu^2)\tilde{w} = 0 \tag{2.35}$$

where

$$\nu = (k^2+l^2)^{1/2}h \tag{2.36}$$

This is Bessel's equation with independent solutions $J_\nu(\zeta)$, $Y_\nu(\zeta)$. As $z\to\infty$, $\zeta\to 0$ and $Y_\nu(\zeta)\to\infty$, so that only Bessel functions of the first kind are appropriate in the infinite-domain

case. To compare with the uniformly stratified case we state the solutions in unbounded and bounded domains:

for an unbounded domain:

$$\tilde{w} = \tilde{w}_0 \frac{J_\nu(\zeta)}{J_\nu(\zeta_0)} \tag{2.37}$$

for a rigid lid at $z=D$:

$$\tilde{w} = \tilde{w}_0 \frac{J_\nu(\zeta)Y_\nu(\zeta_D) - Y_\nu(\zeta)J_\nu(\zeta_D)}{J_\nu(\zeta_0)Y_\nu(\zeta_D) - Y_\nu(\zeta_0)J_\nu(\zeta_D)} \tag{2.38}$$

Here, ζ_0 and ζ_D are the values of ζ at $\zeta=0$ and $\zeta=D$; ie,

$$\zeta_0 = \frac{N_0 h}{U}, \qquad \zeta_D = \zeta_0 e^{-D/h} \tag{2.39}$$

The case of decaying stratification differs from that of uniform N in a number of important respects. Firstly, and perhaps surprisingly, the infinite domain case admits resonance modes - at those values of (k,l) for which

$$J_\nu(\zeta_0) = 0 \tag{2.40}$$

This can occur because the waves cannot propagate above a certain height and so (most of) their energy remains trapped in the region where $N>|k|U$. The path along which wave energy propagates may be determined by the technique of *ray-tracing* (Lighthill, 1978) - similar to geometric optics - where this path is that of a particle moving with the local group velocity. In this case the path is cusped (Figure 2.2). Mathematically, resonance is possible for some modes if

$$\frac{N_0 h}{U} > j_{0,1} \tag{2.41}$$

where $j_{0,1}$ is the smallest positive root of $J_0(x)=0$. Informally, this occurs if the approach flow is "sufficiently stratified" over "sufficient depth".

Secondly, and less surprisingly, when D/h is large the rigid-lid case becomes (for fixed z) a

closer and closer approximation to the unbounded solution. To see this, rewrite (2.38) as

$$\tilde{w} = \tilde{w}_0 \frac{J_\nu(\zeta)}{J_\nu(\zeta_0)} \left(\frac{1 - Y_\nu(\zeta) J_\nu(\zeta_D)/Y_\nu(\zeta_D)}{1 - Y_\nu(\zeta_0) J_\nu(\zeta_D)/Y_\nu(\zeta_D)} \right) \tag{2.42}$$

and, since $Y_\nu(\zeta_D) \to \infty$ as $D/h \to \infty$, whilst $|J_\nu| < 1$, the bracketed term tends to unity for fixed z.

The basic difference between the two types of stratification can be summed up by saying ... *for uniform stratification it is the rigid lid which confines the wave energy, whilst, for decaying stratification, it is the density profile itself.*

The literature contains many attempts to construct a non-reflecting upper boundary condition in order to simulate what happens in an infinite domain. These tend to fall into one of three classes.

(i) *Absorbing layer*; eg Clark and Peltier (1984). Employ a damping region of high artificial viscosity/Rayleigh friction. Actually, it could be argued that one of the best sources of artificial viscosity is a coarse grid.

(ii) *Solution of a (one-dimensional) wave equation*; eg Orlanski (1976), Miller and Thorpe (1981), Han et al. (1983). For steady flows the upper boundary condition is:

$$U \frac{\partial \phi}{\partial x} + c_z \frac{\partial \phi}{\partial z} = 0 \qquad \text{on } z = z_{max} \tag{2.43}$$

The vertical phase velocity c_z is either specified externally or, more commonly, determined from the discretised derivatives at interior nodes. The rationale behind the scheme is that (2.43) admits travelling waves of the form $e^{ik(z - c_z x/U)}$ which, by restricting c_z to positive values, allows outward-travelling waves only. An additional Courant-type restriction $c_z \Delta x / U \Delta z \leq 1$ is required for stability.

There are serious conceptual difficulties with applying this to *dispersive* (phase-

velocity-dependent-on-wavenumber) systems - such as internal gravity waves. Wave energy propagates with the group velocity $\vec{c}_g$, not the phase velocity $\vec{c}_p$. As we have already noted, the phase velocity and group velocity are at right angles in a frame moving with the mean wind (Figure 2.1). Since the vertical components have opposite signs and the radiation condition implies a group velocity pointing upward, then, by contrast with the assumption implicit in (2.43), the vertical component of the phase velocity is actually *negative*.

(iii) *Klemp and Durran's method;* Klemp and Durran (1983). The linearised theory of internal waves is used to link boundary values of outflow velocity and pressure perturbation (or perhaps, more usefully, $\partial w/\partial z$ and $\partial p/\partial z$). For a linearised, Boussinesq system with uniform upstream velocity and constant density gradient, the pressure perturbation and vertical velocity perturbation are proportional (and in phase) in wavenumber space:

$$\tilde{p} = \frac{\sqrt{N^2 - k^2 U^2}}{\sqrt{k^2 + l^2}} \rho_0 \tilde{w} \tag{2.44}$$

Klemp and Durran (1983) analyse in detail the slightly simpler two-dimensional (l=0) hydrostatic case ($|k|U \ll N$):

$$\tilde{p} = \frac{N}{|k|} \tilde{w} \tag{2.45}$$

For propagating modes the radiation condition fixes the sign on the RHS of (2.44) or (2.45). In Klemp and Durran's scheme, w is computed on the boundary (by continuity), then Fourier transformed. The value of the pressure perturbation on the boundary is then recovered by inverse-transforming (2.45).

The rigid-lid approximation is fairly extreme in the atmospheric context and, in practice, an elevated inversion (rapid rise in temperature with height) can be treated as a discontinuity, with wave or exponential solutions on either side as before, $\tilde{w}$ continuous and a jump in $d\tilde{w}/dz$ given by integrating equation (2.17) across the inversion:

$$\left[\frac{d\tilde{w}}{dz}\right]_{h_i^-}^{h_i^+} = -\left(\frac{k^2+l^2}{k^2}\right)\frac{1}{F_i^2}\frac{\tilde{w}(h_i)}{h_i} \tag{2.46}$$

where

$$F_i = \frac{U}{\sqrt{gh_i\Delta\rho/\rho_0}} \tag{2.47}$$

is the Froude number of the inversion at height h_i. Complete solutions for this and other potential-temperature/density profiles have been given by Hunt et al. (1988b).

2.2.2 Finite-Amplitude Models

Long's Model

Unlike linearised theory, the model of Long (1953) makes no assumption of small-amplitude perturbations, but is applicable to finite-amplitude *two-dimensional, steady, incompressible, inviscid flow with no closed streamlines*. A finite-amplitude solution is possible under these circumstances because of the absence in two-dimensional flows of vorticity enhancement by vortex-line stretching, so that, without viscous diffusion of vorticity generated at the boundary, the only source of vorticity is that generated baroclinically. The derivation given below is more compact than Long's original and demonstrates how his model equation emerges from the vorticity equation integrated along a streamline.

In steady flow the incompressibility condition $\vec{U}\bullet\nabla\rho=0$ implies that ρ is constant along streamlines. Hence, in two dimensions, $\rho=\rho(\psi)$, where $\psi(x,z)$ is the stream-function, such that

$$U = \frac{\partial\psi}{\partial z} \qquad W = -\frac{\partial\psi}{\partial x} \tag{2.48}$$

The inviscid Navier-Stokes equation can be written (without the Boussinesq approximation) as

$$\rho[\nabla(\tfrac{1}{2}\vec{U}^2) - \vec{U}\wedge(\nabla\wedge\vec{U})] = -\nabla P + \rho\vec{g} \tag{2.49}$$

Taking the curl, we eliminate pressure and deduce an equation for the vorticity $\vec{\omega}=\nabla\wedge\vec{U}$:

$$\rho\vec{U}\bullet\nabla\vec{\omega} = \vec{\omega}\bullet\nabla(\rho\vec{U}) - \nabla\rho\wedge\nabla(gz+\tfrac{1}{2}\vec{U}^2) \tag{2.50}$$

In two dimensions, $\vec{\omega}=(0,\nabla^2\psi,0)$, so that $\vec{\omega}\bullet\nabla(\rho\vec{U})=0$, whilst

$$(\nabla\rho\wedge\nabla)_2 = \frac{\partial\rho}{\partial z}\frac{\partial}{\partial x}-\frac{\partial\rho}{\partial x}\frac{\partial}{\partial z} = \frac{d\rho}{d\psi}\left(\frac{\partial\psi}{\partial z}\frac{\partial}{\partial x}-\frac{\partial\psi}{\partial x}\frac{\partial}{\partial z}\right) = \frac{d\rho}{d\psi}\vec{U}\bullet\nabla \tag{2.51}$$

Hence, since ρ and its derivatives commute with $\vec{U}\bullet\nabla$, equation (2.50) becomes

$$\rho\vec{U}\bullet\nabla[\omega_2 + \frac{1}{\rho}\frac{d\rho}{d\psi}(gz + \tfrac{1}{2}\vec{U}^2)] = 0 \tag{2.52}$$

The square-bracketed quantity is therefore constant along streamlines. Substituting for ω_2, we obtain the equation

$$\nabla^2\psi + \frac{1}{\rho}\frac{d\rho}{d\psi}[gz + \tfrac{1}{2}(\nabla\psi)^2] = f(\psi) \tag{2.53}$$

where $f(\psi)$ is to be deduced from conditions far upwind; (here we require the assumption of no closed streamlines).

A more convenient formulation is in terms of the streamline displacement δ. Assuming that, far upwind, there exists a plane-parallel undisturbed flow with

$$U_\infty \equiv U(z_\infty) = \frac{d\psi}{dz_\infty} \tag{2.54}$$

then we may change variables from ψ to z_∞ (the upstream height of the streamline) and write equation (2.53) as

$$\nabla^2 z_\infty - \left(\frac{N}{U}\right)_\infty^2 (z - z_\infty) + \tfrac{1}{2}\left[(\nabla z_\infty)^2 - 1\right]\frac{d}{dz_\infty}\ln(\rho U_\infty^2) = 0 \tag{2.55}$$

where $N^2 = -\frac{g}{\rho}\frac{d\rho}{dz_\infty}$. Finally, we may deduce from this Long's equation for the streamline displacement $\delta = z - z_\infty$:

$$\nabla^2 \delta + \left(\frac{N}{U}\right)_\infty^2 \delta - \tfrac{1}{2}\left[(\nabla\delta)^2 - 2\frac{\partial\delta}{\partial z}\right]\frac{d}{dz_\infty}\ln(\rho U_\infty^2) = 0 \tag{2.56}$$

The last term on the LHS vanishes if ρU_∞^2 is independent of height (or, under the Boussinesq approximation, for constant U_∞) and with this simplification Long's model reduces to the linear equation

$$\nabla^2 \delta + \left(\frac{N}{U}\right)_\infty^2 \delta = 0 \tag{2.57}$$

with δ conveniently given on the boundaries by the shape of the surface. Important solutions of (2.57) for flow over obstacles were obtained by H.E. Huppert and J.W. Miles in a classic series of papers, of which Huppert and Miles (1969) may serve as a good example.

Yih (1965) derived a modified form of equation (2.53):

$$\nabla^2 \psi' + \frac{1}{\rho_0}\frac{d\rho}{d\psi'} g z = f(\psi') \tag{2.58}$$

by first making the inertial transformation

$$\vec{U}' = \left(\frac{\rho}{\rho_0}\right)^{1/2} \vec{U} \tag{2.59}$$

with ρ_0 a constant density, so that, in incompressible flow, $\rho\vec{U}\bullet\nabla\vec{U} = \rho_0\vec{U}'\bullet\nabla\vec{U}'$. The inertial effect of density is then removed, so that the inviscid equations take a form similar to those with the Boussinesq asumption.

Despite the advantage of allowing finite-amplitude motions, Long's model founders on the requirement that steady-flow conditions be realised upstream at infinity and, as MacIntyre

(1972) has shown by a weakly non-linear analysis, this cannot be the case for subcritical flow confined between parallel planes, since (in the absence of dissipation) transient modes will propagate upstream indefinitely.

Breaking Waves and Severe Downslope Windstorms

The breaking of internal gravity waves forced by two-dimensional topography has been extensively investigated, not least because of its association with severe downslope windstorms. This association was apparently first stated explicitly by Clark and Peltier (1977) and contrasting mechanistic descriptions of the phenomenon have been proposed by Clark and Peltier (1984) and Smith (1985). Whilst both recognised the importance of the wave-breaking (ie, isentrope-overturning) region as a critical layer, the mathematical formalism and prediction of the critical height(s) for resonance differ.

Clark and Peltier's (1984) hypothesis - based on a linear analysis - postulated that the wave-breaking region acts as a reflector and is arranged such that the space between the breaking layer and the ground is a resonant cavity for internal waves. They tested this hypothesis (indirectly) by computing the time-dependent behaviour of the flow over a two-dimensional bell-shaped hill with an artificially fixed critical layer (in this case, a mean-flow reversal) at different heights. The main criticisms brought to bear on Clark and Peltier's mechanism are the validity of the linearisation and the lack of any theoretical justification for why the critical layer should act as a perfect *reflector*, with the phase of the reflected waves such as to cause constructive interference.

By contrast, Smith (1985) integrated the fully non-linear Long's model equation to demonstrate the possibility of strong downslope flow beneath a deep stagnant layer of well-mixed fluid. The formal analogy between Smith's model and the hydraulic transition from subcritical (deep layer with weak flow) to supercritical (shallow layer with strong flow) - see Figure 2.3 - has been drawn by Durran and Klemp (1987) and Bacmeister and Pierrehumbert (1988).

Predictions of z_c, the height of the critical layer for resonance, differ between the two models: Clark and Peltier's model predicts resonance at discrete values such that $Nz_c/U=(n+½)\pi$, whereas Smith's model admits resonance over broad ranges $(2n+1/2)\pi<Nz_c/U<(2n+3/2)\pi$. Thus, it should be possible to distinguish between the two mechanisms by a suitably designed experiment. Such experiments have been carried out numerically by Bacmeister and Pierrehumbert (1988) and experimentally (in a stratified towing tank) by Rottman and Smith (1989), both coming out broadly in favour of Smith's model, though with some qualifications related to the idealisations involved.

The asymmetric flow field characterised by strong downslope winds in the lee is also associated with a high-drag state. (The two are intimately connected by Bernoulli's Theorem.) The stages in the temporal approach to this "mature-windstorm" state have been investigated by Scinocca and Peltier (1993) using a three-stage, nested-grid simulation.

Whilst we now have good reason to recognise breaking internal waves as a primary cause of the high-drag/severe-downslope-windstorm state the circumstances under which topographically forced gravity waves do actually break are far less well established. Huppert and Miles (1969) solved Long's equation for steady, stratified flows over two-dimensional obstacles with semi-elliptical cross-section and computed the critical Froude number at which the flow first becomes statically unstable - a vertical streamline appearing in the flow - interpreted as the point at which the lee waves begin to break. Beyond this point Long's model is no longer valid. Their calculations indicate critical Froude numbers of order unity, increasing monotonically as the streamwise extent of the obstacle increased, but dependent, in part, upon body shape. Stratified towing tank studies of the lee wave structure over three-dimensional obstacles have been carried out with short triangular ridges by Castro et al. (1983) and Castro (1987), cosine-squared ridges by Rottman and Smith (1989) and various three-dimensional hills by Castro and Snyder (1993). These experiments confirmed that steady wave breaking could occur (typically, in a range $0.2<Fr<Fr_{crit}$) with wave amplitude maximised by "tuning" the body shape to the lee-wave field. The experiments generally support the contention that Fr_{crit} increases as streamwise length or spanwise width increase.

2.2.3 Low-Froude-Number Flows

In stably stratified flow fluid elements must acquire potential energy in order to rise over an obstacle. They can do so in two ways:

- by sacrificing their own kinetic energy;
- by pressure and viscous interaction with neighbouring fluid elements.

The energy argument exploited by Sheppard (1956) and extensively tested by Snyder et al. (1985) assumes that the second source of energy is negligible and postulates the existence in sufficiently stable flow of an upstream height - the *dividing-streamline height* - below which fluid has insufficient energy to attain the summit of the hill and must pass around the sides. This concept is analogous to a ball rolling up a hill, gaining height at the expense of its kinetic energy. The dividing-streamline height calculated in this way is dependent on the height, but independent of the shape, of the hill.

However, the individual elements of fluid flow are not isolated, but interact through the pressure field. This is the argument of Smith (1989) (and the references contained therein). According to Smith's (linearised, hydrostatic) analysis it is the increased pressure on the upstream face due to a positive density perturbation above which causes upwind flow stagnation. The density field depends on the streamline displacement over the hill and, consequently, is dependent on hill shape.

Let us see where the disagreement emerges.

Bernoulli's Theorem for incompressible, inviscid flow gives for conditions on a streamline:

$$\tfrac{1}{2}\vec{U}^2 + gz + \frac{P}{\rho_\infty} = \tfrac{1}{2}U_a^2(z_\infty) + gz_\infty + \frac{P_a(z_\infty)}{\rho_\infty} \qquad (2.60)$$

where ambient profiles of pressure and velocity are denoted by subscript a and conditions on the streamline far upwind by subscript ∞. The pressure difference can be broken down into the departure from the ambient pressure at the same height, $P^*=P-P_a(z)$, and the difference in ambient pressure (assumed hydrostatic) between the two heights; thus:

$$
\begin{aligned}
P - P_a(z_\infty) &= P - P_a(z) + P_a(z) - P_a(z_\infty) \\
&= P^* - \int_{z_\infty}^{z} \rho_a(z')g\,dz' \\
&= P^* - \rho_\infty g(z - z_\infty) - \int_{z_\infty}^{z} (\rho_a(z') - \rho_a(z_\infty))g\,dz' \\
&= P^* - \rho_\infty g(z - z_\infty) - \int_{z_\infty}^{z} \frac{d\rho_a}{dz'} g(z - z')\,dz'
\end{aligned}
\tag{2.61}
$$

Substituting in (2.60) and rearranging gives

$$
\tfrac{1}{2}(U_\infty^2 - U^2) = \frac{P^*}{\rho_\infty} + \int_{z_\infty}^{z} (z - z')N^2(z')\,dz' \tag{2.62}
$$

where $N^2 = -\frac{g}{\rho_\infty}\frac{d\rho_a}{dz}$. In words, the fluid loses kinetic energy and gains an equal amount of potential energy: part as pressure energy, part as gravitational energy. Incipient stagnation (U=0) must occur somewhere on the front face if there exists a positive height H_c, less than the hill height H, such that

$$
\tfrac{1}{2}U_a^2(H_c) = \frac{P^*}{\rho_\infty} + \int_{H_c}^{H} (H - z')N^2(z')\,dz' \tag{2.63}
$$

Equations (2.62) and (2.63) simplify considerably if one assumes uniform upstream velocity U_∞ and buoyancy frequency N. Bernoulli's equation then gives

$$
\tfrac{1}{2}(U_\infty^2 - U^2) = \frac{P^*}{\rho_\infty} + \tfrac{1}{2}N^2\delta^2 \tag{2.64}
$$

where $\delta = z - z_\infty$ is the streamline displacement. The equation for H_c becomes

$$
\tfrac{1}{2}U_\infty^2 = \frac{P^*}{\rho_\infty} + \tfrac{1}{2}N^2(H - H_c)^2 \tag{2.65}
$$

If P^*=0 - ie, the pressure is everywhere equal to the ambient pressure at the same height - then (2.65) gives:

$$H_c = H(1-Fr) \tag{2.66}$$

where $Fr=U_\infty/NH$ is the hill Froude number. Upwind stagnation is, therefore, expected to take place if the Froude number is less than a critical value of unity.

The main criticism brought to bear on the dividing-streamline formulation, $H_c=H(1-Fr)$, is that it assumes that $P^*=0$; ie, that the pressure is everywhere equal to the ambient pressure at the same height. Smith (1989) shows that one component of P^* cancels with the streamline-displacement part of (2.64). Invoking the hydrostatic assumption ($\partial P/\partial z=-\rho g$):

$$\frac{\partial \boldsymbol{P}^*}{\partial z} = -(\rho(z)-\rho_a(z))\boldsymbol{g} = -(\rho_a(z_\infty)-\rho_a(z))\boldsymbol{g} = -\rho_\infty N^2\delta(z_\infty) \tag{2.67}$$

so that

$$\frac{1}{\rho_\infty}\frac{\partial \boldsymbol{P}^*}{\partial z_\infty} = -N^2\delta(z_\infty)\frac{\partial z}{\partial z_\infty} = -N^2\delta(1+\frac{\partial \delta}{\partial z_\infty}) \tag{2.68}$$

and hence

$$\frac{\boldsymbol{P}^*}{\rho_\infty} = N^2\int_{z_\infty}^{\infty}[\delta+\frac{\partial}{\partial z_\infty^{/}}(\tfrac{1}{2}\delta^2)]\,dz_\infty^{/} = N^2(I_\delta - \tfrac{1}{2}\delta^2) \tag{2.69}$$

where I_δ is essentially determined by the density perturbation above:

$$I_\delta = \int_{z_\infty}^{\infty}\delta(x,y,z^{/})\,dz^{/} \tag{2.70}$$

On this basis, the height-dependent term $\tfrac{1}{2}N^2\delta^2$ cancels out (which nullifies Sheppard's energy argument), and the critical height becomes dependent on hill shape. Exploiting linearised hydrostatic theory, Smith goes on to show, for a particular class of axisymmetric hills ("Witch of Agnesi" shape in cross-section), that surface stagnation does not occur until a critical Froude number of 0.77 is reached and, in many cases, may be preceded by stagnation aloft.

There are some conceptual difficulties with Smith's theory - not least the use of *linearised*

theory to predict stagnation (which must be an example of an O(1) perturbation if ever there was one) and the use of the *hydrostatic* approximation for hills of reasonable slope.

Let us rearrange the energy balance equation (2.65):

$$H_c = H - \frac{U_\infty}{N}\left(1 - \frac{P^*}{\frac{1}{2}\rho_\infty U_\infty^2}\right) \tag{2.71}$$

Now P^* may not be zero, but, since the flow must diverge laterally to flow around the hill, it is *very difficult to see how it can be negative*. Since kinetic energy must be sacrificed to increase both pressure and gravitational potential energy, then, if anything, the critical Froude number for upwind stagnation could well be greater than unity.

Despite the unresolved controversy, the dividing-streamline concept has largely been confirmed in the laboratory, (the case for the defence is summed up in Snyder et al., 1985), and, as a result, it has been embodied in the US Environmental Protection Agency's dispersion modelling code CTDMPLUS (Perry, 1992).

The assumption that at very low Froude numbers flow is compelled to move in roughly horizontal planes is implicit in the work of Drazin (1961), further extended by Brighton (1978) to allow for non-uniform approach flow $U_a(z)$. The basis of this model is as follows.

(1) In strongly stable flow around an isolated obstacle, the flow moves approximately horizontally, except in zones of thickness $\alpha_1 FrH$ and $\alpha_2 FrH$ at the bottom [B] and top [T] of the hill; (see Figure 2.4).

(2) In [H1] and [H2] the horizontal velocity is described by two-dimensional potential theory.

(3) Horizontal pressure gradients must vary with z because of variations in $U_a(z)$ and the radius of the topography. Hence, the vertical pressure gradient is perturbed and is balanced by perturbations to density gradients produced by small vertical displacements of streamlines in [H1].

(4) Streamlines pass through [T] and over the top if their initial height is greater than $H(1-\alpha_2 Fr)$.

Formally, Drazin's approach is to expand the inviscid equations of motion in powers of Fr^2. The leading-order solutions are asymptotic expansions in the limit as $Fr \rightarrow 0$.

Finally, one must ask whether the analysis and issues raised above represent purely mathematical exercises or have practical significance. A relatively moderate potential-temperature gradient of one degree per hundred metres gives a buoyancy frequency N=0.02s^{-1}, which, together with an equally representative wind speed U=10 m s^{-1}, yields a Froude number of unity for a topographic height of a mere 500m. Thus, it is clear that low Froude numbers are often attained in atmospheric flows. Looked at from another viewpoint, many atmospheric flows will have Froude numbers of order unity where neither asymptotic low or high-Froude-number theories are valid. I think this represents something of a challenge.

2.2.4 Turbulent Flow Over Low Hills

Although it has undergone considerable refinement, the Jackson and Hunt (1975) theory for two-dimensional boundary layer flow over a small hump remains the foundation of most linearised models of turbulent air flow over low hills. The main elements of the model are as follows.

(1) The flow is divided into an *inner* layer (of vertical scale ℓ) where the perturbation shear stress is dynamically significant and an *outer* layer where the perturbation is essentially inviscid.

(2) Turbulence closure in the inner layer is effected by a simple mixing-length model.

(3) In each layer the equations of motion are linearised by writing the mean velocity as the sum of the upstream velocity and a small perturbation. (Formally, these are the zeroth and first order terms in matched asymptotic expansions.)

(4) The linearised equations are Fourier-transformed in the horizontal and analytical solutions obtained in wavenumber space.

(5) The Fourier transforms are inverted (numerically) to obtain the velocity field.

Figure 2.5 illustrates the mechanisms by which the flow perturbation is generated. The forced displacement of streamlines, in conjunction with any ambient stratification, generates an outer-

layer pressure field. This, in turn, drives an accelerated flow at lower levels, which is modified by the effects of turbulent transport and surface roughness.

This mechanistic description indicates the form of the flow perturbation in each layer. In the inner layer the "basic" velocity is the upwind velocity displaced by the local surface height $z=Hf(x/L)$. Thus,

$$U = U_a(Z) + \epsilon U_a(\ell)\hat{u}(\frac{x}{L},\frac{Z}{\ell}) , \qquad W = \frac{H}{L}f'(\frac{x}{L})U + \epsilon U_a(\ell)\frac{\ell}{L}\hat{w}(\frac{x}{L},\frac{Z}{\ell}) \tag{2.72}$$

where $Z=z-Hf(x/L)$ is the height above the surface, whilst, in the outer layer:

$$U = U_a(z) + \frac{H}{L}U_a(L)\hat{u}(\frac{x}{L},\frac{z}{L}) , \qquad W = \frac{H}{L}U_a(L)\hat{w}(\frac{x}{L},\frac{z}{L}) \tag{2.73}$$

L is the horizontal scale of the hill (for example, the half-length or the inverse mean wavenumber). The inner-layer height ℓ ($\ll L$) and small parameter ε, which determines the magnitude of the inner-layer perturbation, emerge naturally from the analysis which follows.

Since pressure is essentially uniform across the thin inner layer (the *boundary layer approximation*), whilst the longitudinal pressure gradient is comparable with the inertial acceleration terms in each layer, we have

$$\frac{\Delta P}{L} \sim \frac{\epsilon U_a^2(\ell)}{L} \sim \frac{H}{L}\frac{U_a^2(L)}{L} \tag{2.74}$$

and hence

$$\epsilon = \frac{H}{L}\left(\frac{U_a(L)}{U_a(\ell)}\right)^2 \tag{2.75}$$

(My definition of ε differs from Jackson and Hunt. My $\varepsilon U_a(\ell)$ replaces their εu_*. This has two benefits: it removes the necessity of assuming the precise form of the upstream profile $U_a(z)$, thereby reducing the surfeit of logarithms in the mathematical analysis, and it more clearly illustrates the different advection velocities $U_a(\ell)$ and $U_a(L)$ in the two layers.)

It remains to specify the inner-layer scale ℓ. This depends in part upon the turbulence closure. Since, by assumption, the inner layer is that region in which the shear-stress divergence is of comparable magnitude with the inertial terms, we have

$$U_a(\ell)\frac{\Delta u}{L} \sim \frac{\Delta \tau}{\ell} \tag{2.76}$$

where Δu and $\Delta\tau$ are the magnitudes of velocity and shear-stress perturbations. On the other hand, τ and u are related to each other by a turbulence-closure assumption. The mixing-length closure is

$$T_{xZ} = \kappa^2 Z^2 \left|\frac{\partial U}{\partial Z}\right| \frac{\partial U}{\partial Z} \tag{2.77}$$

which, on linearising and subtracting the upstream balance ($\tau_0=\kappa u_* Z$), yields

$$\tau_{xZ} = 2\kappa u_* Z \frac{\partial u}{\partial z} \tag{2.78}$$

from which we have the order-of-magnitude balance:

$$\Delta\tau \sim 2\kappa u_* \Delta u \tag{2.79}$$

Combining (2.76) and (2.79) we obtain an implicit equation for the inner-layer scale ℓ:

$$\frac{\ell}{L}\ln(\ell/z_0) \sim 2\kappa^2 \tag{2.80}$$

A number of authors have questioned (2.79) arguing that for equilibrium turbulence the perturbation velocity is logarithmic, so that $Z\frac{\partial u}{\partial Z} \sim \frac{\Delta u}{\ln(\ell/z_0)}$ and (2.80) should be replaced by

$$\frac{\ell}{L}\ln^2(\ell/z_0) \sim 2\kappa^2 \tag{2.81}$$

However, this *inner surface layer* (Hunt et al., 1988a) is that effectively zero-pressure-gradient layer immediately adjacent to the surface, which, whilst it may be important for characterising turbulent fluxes to the surface, plays no dynamical role in an inner-layer flow driven by the

pressure gradient developed in the outer layer.

The Jackson-Hunt model was extended to three dimensions by Mason and Sykes (1979a). Subsequently, model development diverged and different organisations produced computer software for the application of the theory to real terrain.

An acknowledged failing of the original theory was that, although pressure and vertical velocity matched between inner and outer layers, there was a mismatch in the longitudinal velocity, essentially because the leading-order solutions in the two layers corresponded to different advection-velocity scales $U_a(\ell)$ and $U_a(L)$. Two different practical solutions were advanced: the introduction of an intermediate region of approach-flow velocity shear and a wavenumber-dependent blending strategy.

Hunt et al. (1988a,b) subdivided the inviscid outer layer into an *upper* layer, where the approach-flow velocity is essentially uniform but stratification is important, and a comparatively thin *middle* layer, where the effect of approach-flow velocity shear is manifested. The leading-order solutions for each layer were incorporated into the code FLOWSTAR (Carruthers et al., 1991).

The alternative approach was adopted by Taylor et al. (1983) in their code MS3DJH (**M**ason and **S**ykes' **3**-**D**imensional extension of **J**ackson-**H**unt theory: a deferential but not very imaginative acronym!). They argued that, instead of a single horizontal length scale L, real terrain could be regarded as made up of a large range of scales, and they introduced the concept of wavenumber scaling. A universally valid solution is formed (in Fourier space) by blending inner- and outer-layer solutions with different horizontal scales, $L_k=2\pi/k$, inner-layer length scales, ℓ_k, and inner- and outer-layer velocity scales, $U_a(c_1\ell_k)$ and $U_a(c_2L_k)$ respectively. For each wavenumber, the blending function is a simple function of Z/ℓ_k.

Both field studies (Bradley, 1983) and wind-tunnel measurements (Britter et al., 1981) indicate that changes in surface roughness may have a significant effect on wind speed in the inner layer. (This represents something of a challenge in the wind tunnel, where the requirement that the surface be aerodynamically rough often demands that individual

roughness elements be of a size out of all proportion with geometric similarity considerations, and, as noted in the second reference above, may preclude direct measurements in the inner layer). Flow perturbations due to surface roughness modulation can also be treated by linearised theory (Walmsley et al., 1986; Belcher et al., 1990). To leading order, it may be shown that a varying surface roughness is equivalent to a uniformly rough surface with variable surface tangential velocity, and, moreover, that the flow perturbations so induced may be added linearly to those brought about by height variations. Roughness-induced perturbations have been included in both FLOWSTAR and MS3DJH/3R codes.

The description of turbulence in the above models is fairly rudimentary and, although the mixing-length model has been confirmed to serve its purpose for mean-flow calculations, a more advanced model is required to predict turbulence statistics - for example, in dispersion calculations. The basis of the MSFD (**M**ixed **S**pectral **F**inite-**D**ifference) model of Beljaars et al. (1987), or its personal-computer implementation MS-MICRO, was to combine the spectral approach in the horizontal with a finite-difference solution in the vertical, thus allowing a more general turbulence model. They used both a linearised k-ε model and an algebraic-stress k-ε-τ model (subsequently corrected by Walmsley and Padro, 1990) to compute mean flow and turbulence over the Askervein hill. Although a finite-difference calculation in the vertical replaces the analytical solution arising from the mixing-length model, the additional computational overheads are not large, since it is no longer necessary to compute the Bessel functions which arise in the earlier model. A non-linear extension of MSFD has been described by Xu and Taylor (1992).

2.2.5 Dispersion Modelling in Complex Terrain

Although complex computational models have been used for dispersion calculations (for example, the Reynolds-stress modelling of El Tahry et al., 1981, the large-eddy simulations of Nieuwstadt and van Harem, 1988 and the random-walk model of Thomson, 1986), most dispersion modelling for routine and regulatory use is still done with simple analytical schemes - the majority with some form of gaussian-plume model. The reasons for this are that such models are quick and easy to apply, require few input parameters, little expert

knowledge, small computer resources and (for probabilistic risk assessment and long-term averages) can cover a large matrix of cases comparatively quickly. But, before we write ourselves out of a job, we must remark that their simplicity is only suited to calculations in well-defined boundary layers and over homogeneous terrain. The assumptions of straight-line advection with well-defined spreading rates are clearly contravened in complex topography.

The simplest model for downwind concentrations from a point source makes use of little more than the conservation of material, yet is of some practical use in estimating concentrations from sources located in well-mixed regions, such as recirculating flow or once the plume has expanded to fill the boundary layer. For a steady emission of Q units s^{-1}, an equal amount of material must pass through any downwind cross-stream plane each second. Assuming material to be uniformly spread over crosswind area A and advected downwind at speed U, then $Q=CUA$ or

$$C_{av} = \frac{Q}{UA} \tag{2.82}$$

We can improve the model without losing the basic physical constraint of material conservation by admitting a varying crosswind profile (typically a gaussian distribution):

$$C(x,y,z) = \frac{Q}{2\pi U\sigma_y\sigma_z} e^{-\frac{1}{2}y^2/\sigma_y^2} e^{-\frac{1}{2}(z-z_p)^2/\sigma_z^2} \tag{2.83}$$

where σ_y and σ_z represent rms plume spread in lateral (y) and vertical (z) directions about the plume centreline at height z_p. Since the plume cannot expand downwards indefinitely, the presence of a lower boundary may be incorporated through the use of an additional "reflected" plume:

$$C(x,y,z) = \frac{Q}{2\pi U\sigma_y\sigma_z} e^{-\frac{1}{2}y^2/\sigma_y^2}\left(e^{-\frac{1}{2}(z-z_p)^2/\sigma_z^2} + e^{-\frac{1}{2}(z+z_p)^2/\sigma_z^2}\right) \tag{2.84}$$

so that the integrated flux of material is still Q and the no-flux condition at the boundary ($\partial C/\partial z=0$ on $z=0$) is satisfied. Additional reflection terms can be added for an elevated inversion layer. Removal of material at the ground or by incorporation in rainwater can be achieved by making the plume strength Q a function of distance downwind.

The gaussian plume model (2.84) has been widely used for dispersion modelling. In the UK the definitive version was, for a long time, the R91 model (Clark, 1979), whose title gives undue weighting to the NRPB's report-numbering system. The basic model requires little more than the wind speed at one height and an (often subjective) categorisation of atmospheric stability ranging from A (very unstable) to G (very stable) with specified functional forms of $\sigma_y(x)$ and $\sigma_z(x)$ (the *Pasquill-Gifford curves*) for each category. Modifications to incorporate additional effects such as deposition, plume buoyancy, etc. were detailed in a subsequent set of reports, summarised by Jones (1986).

Recently, attention has been focused on a new generation of dispersion models which seek to overcome some of the known deficiencies of R91 and related schemes. An important example is UKADMS (**U**nited **K**ingdom **A**tmospheric **D**ispersion **M**odelling **S**ystem) described by Hunt et al. (1990). The objectives of the new model were:

- to provide standardisation by making model parameters continuous functions of measurable (or derivable) physical quantities, rather than the subjective and ambiguous use of discrete dispersion categories;
- to incorporate better understanding of the mean and turbulence structure of the atmospheric boundary layer (so that, for example, the plume spread parameters σ_y and σ_z may be functions of plume height and, in convective conditions, the plume crosswind profile is non-gaussian);
- to incorporate information now routinely available from meteorological measurements (such as the mixing height), rather than basing the entire scheme on surface-layer meteorology;
- to include complex effects associated with the source (plume buoyancy; proximity of buildings), complex terrain (topography; coastlines; urban boundaries) removal processes (deposition; radioactive decay) and, in addition to the mean concentration, to make some estimate of concentration fluctuations and an assessment of error.

The integrated UKADMS model can be run on a small personal computer.

The main effects of topography on plume dispersion are changes to the mean flow (which affects the plume path), turbulence (which affects the rate of spread) and the possibility of advection into recirculating flow regions. Topographic effects on diffusion have been

reviewed by Egan (1975, 1984).

Of the parameters in the gaussian-plume model (2.84) the maximum ground-level concentration is most sensitive to the plume height z_p. To see this, we note that the ground-level centre-line concentration is given by

$$C = \frac{Q}{\pi U \sigma_y \sigma_z} e^{-\frac{1}{2} z_p^2/\sigma_z^2} \tag{2.85}$$

and, assuming that $\sigma_y = \gamma\sigma_z$, this can be written

$$C = \frac{Q}{U z_p^2} f\left(\frac{z_p}{\sigma_z}\right) \qquad \text{where} \qquad f(\zeta) = \frac{1}{\gamma\pi}\zeta^2 e^{-\frac{1}{2}\zeta^2} \tag{2.86}$$

The maximum concentration (occurring at $\zeta = z_p/\sigma_z = \sqrt{2}$) is

$$C_{max} = \frac{Q}{U z_p^2} \cdot \frac{1}{\gamma \pi e} \tag{2.87}$$

so that C_{max} is inversely proportional to the square of the plume height. (Whilst this analysis is for a gaussian-plume profile, the last assertion remains true whenever the plume shape is independent of the source height). Thus, for non-separated flow the most important effect of topography is to bring the plume closer to the ground.

The simplest schemes accounting for topographic effects are "deflection" models - that is, they make some assumption about the effective plume height relative to the terrain. Examples of this type include the United States Environmental Protection Agency's models CRSTER and its derivatives COMPLEX 1 and COMPLEX 2 (eg Lavery et al., 1981). In strongly stratified flow vertical motions are inhibited. The worst-case situation - that of straight-line impaction on the surface - is embodied in the VALLEY model (Burt, 1977). This has been criticised as grossly pessimistic. The RTDM model (Egan, 1984) uses the dividing streamline concept to discriminate between plumes which pass over a hill from those which impinge on the upwind face (and split to pass around the sides).

In the above models plume deflection has been based purely on local terrain height (and

height contours for the impingement model). Advanced models accept some computational overheads in deriving a wind field, from which the plume path is recovered as a mean streamline. In the United States Environmental Protection Agency's CTDM model (Perry, 1992) the terrain is idealised as a series of ellipsoids and the wind field obtained as the (analytical) potential flow solution; (two-dimensional potential flow below the dividing-streamline height).

In FLOWSTAR-D (Hunt et al., 1988; Weng and Carruthers, 1994) Fourier methods are used to compute a linearised perturbation wind field. (This is the complex terrain module in UKADMS.) The "-D" indicates diffusion and signifies that, not only is the plume path recovered from integrated mean streamlines, but the crosswind diffusion parameters σ_y and σ_z are also obtained by integrating eddy-diffusivity coefficients. Plume spread depends on both the convergence/divergence of mean streamlines (as expressed by $\partial U_s/\partial s$) and the local turbulence intensity, which may be established by a local equilibrium assumption in the inner layer and by rapid-distortion theory in the outer. The model has been extended to include the highly stratified case, with horizontal flow assumed below a dividing streamline. The two-dimensional potential flow solution in this latter region may be obtained for arbitrary hill shapes by the method of Fourier descriptors.

Another approach to defining the mean flow is that of constructing a mass-consistent wind field from observational data. Examples include NOABL and the MATHEW/ADPIC code (Sherman, 1978 - for its application see also Desiato, 1991). Stable stratification is included in the assumptions about the wind speed profile.

All of the models mentioned above embody the "narrow-plume" assumption - that is, the crosswind concentration profile can be determined from spread parameters σ_y and σ_z defined on the plume centreline. Our calculations in Chapter 6 would indicate that, in some circumstances, this may be far from the case.

Steep topography often gives rise to downwind flow separation. Flow reversal has no place in gaussian plume models and an alternative approach is necessary. Using a diffusion equation analysis, Puttock and Hunt (1979) demonstrate that, for sources outside a *two-dimensional*

recirculating flow, concentrations within that region are fairly well-mixed and approximately equal to the average value along the boundary. In strongly stratified flow a similar analysis is appropriate for the wake region below the dividing streamline in the lee of three-dimensional hills. In an idealised model the same *wake-averaging* procedure may be applied to *three-dimensional* recirculating flow regions, although, in these cases, the recirculating flow region is not closed (Hunt et al., 1978) and fluid may enter by advection as well as diffusion. Indeed, the calculations of Mason and Sykes (1979b, 1981) indicate that the former process usually dominates.

Of course, in developing simple dispersion models the existence and boundaries of recirculating flow regions are assumed to be previously defined. One often wonders ... how?

2.3 Numerical Modelling

The first two parts of this review dealt with experimental observation and theoretical models of flow and dispersion in complex terrain. Attention is now focused on the main subject of this research, namely the numerical computation of flow over topography. From a fluid-mechanical standpoint, this means the flow of a deep turbulent boundary layer over a curved surface.

I have found it appropriate in tracing the development of this subject to present an essentially chronological review of the literature. Nevertheless, it is useful to keep in mind an alternative thematic order. Published work in this field varies widely as regards choice of topography (two- or three-dimensional; real or idealised), working variables, turbulence models, coordinate geometry, time-dependent or steady-state, compressible or incompressible, hydrostatic or non-hydrostatic, and inclusion of effects such as stability, rotation, latent heat transport and surface fluxes - besides a whole variety of numerical schemes for discretising and solving the governing equations.

In undertaking this review it has become apparent that the decisive factor in making numerical simulation of airflow over real topography a practical proposition is the

phenomenal increase in speed and core memory of computer hardware in the last two decades. As little as twenty years ago, computations were confined largely to two dimensions. Raithby et al. (1987) and Dawson et al. (1991) used two-equation turbulence models to compute boundary-layer flow over real hills (Askervein and Steptoe Butte) with grids of 20×20×19 and 40×32×32 nodes respectively. Our own computations used grids of up to 70×53×40 nodes on a desktop workstation. Besides allowing more satisfactory resolution of terrain, the use of grids up to $(128)^3$ on modern supercomputers allows direct numerical simulation and the prospect of direct testing of advanced turbulence models (Rodi and Mansour, 1993).

Some of the earliest computations of neutrally stratified boundary-layer flow over two-dimensional topography were undertaken by Taylor and Gent (1974). (Vertical) turbulent transport was determined by a gradient-transfer/eddy-viscosity model based on a transport equation for the turbulent kinetic energy k and an externally specified length scale l_m, a function of the distance from the boundary (in transformed space). Their method depended on a conformal transformation of the flow domain. This rather restrictive requirement was removed by Taylor (1977), who introduced a vertical coordinate transformation based on the local surface height. Horizontal diffusion was incorporated through the tensorially invariant form of the eddy-viscosity model:

$$-(\overline{u_i' u_j'} - \frac{2}{3}k\delta_{ij}) = \nu_t\left(\frac{\partial U_i}{\partial x_j} + \frac{\partial U_j}{\partial x_i}\right) \tag{2.88}$$

The mixing length l_m still depended to some extent on the coordinate transformation employed. Computations were performed for flow over periodic terrain (driven by an upper-level shear stress), isolated hills and curved ramps; the last was compared with available wind-tunnel data. The discretised equations were expressed in non-conservative, finite-difference form, although some effort was made to check the global momentum budget. Converged solutions could not be obtained within a conservative, finite-volume framework, possibly because of instabilities associated with centred differencing of advection terms.

Deaves (1976, 1980) used a simple mixing-length closure

$$\nu_t = l_m^2 \frac{\partial U}{\partial z} \tag{2.89}$$

to compute turbulent flow over two-dimensional low hills. The mixing-length profile was determined by the vertical distance from the surface and the boundary layer height. To reduce the number of flow equations he used stream function and vorticity (or, strictly, ν_t times vorticity), rather than the, now more common, primitive-variable (pressure-velocity) formulation. The first paper used a cartesian mesh but difficulties with the surface boundary condition prompted a move to a surface-fitting coordinate system (Figure 2.6). The inclusion of non-linear advection terms was found to improve on the Jackson-Hunt theory within the inner layer (as judged by comparison with wind-tunnel data), but supported the assumption that the flow in the outer layer could be treated as an inviscid perturbation (for hills not steep enough to provoke flow separation).

Clark (1977) set out a comprehensive description of a three-dimensional, finite-volume flow solver for arbitrary topography and any specified inflow velocity/potential temperature profiles. He used a terrain-fitting curvilinear coordinate transformation:

$$\zeta = \frac{z - z_s(x,y)}{1 - z_s(x,y)/\boldsymbol{D}} \tag{2.90}$$

which applies a uniform vertical stretching dependent on the distance between the local terrain height $z_s(x,y)$ and the computational domain height D. This has substantial benefits in applying the boundary conditions on upper and lower boundaries. Mass, momentum and potential temperature equations were solved, with the anelastic approximation (neglect $\partial\rho/\partial t$ in the continuity equation) applied to filter sound waves. The code was completely non-hydrostatic: that is, a prognostic equation derived from continuity had to be solved for the pressure, rather than simplifying the pressure calculation to a vertical integration of the density field. Amongst other features of the model were the use of Rayleigh friction; ie, an artificial damping term

$$-\rho\vec{U}/\mathbf{T_R} \tag{2.91}$$

(rather than an increased diffusion coefficient) in the momentum equation, with time constant T_R set to finite values in the upper part of the solution domain, to eliminate wave reflection

from the upper boundary. A non-reflecting outflow radiation condition was used to suppress reflection from the downstream boundary in time-dependent calculations. Subgrid-scale turbulent stresses were parameterised according to Smagorinsky's (1963) model, familiar to the proponents of large-eddy simulation,

$$\tau_{ij} = 2\nu_t(S_{ij} - \frac{1}{3}S_{kk}\delta_{ij}) \tag{2.92}$$

where $S_{ij} = \frac{1}{2}\left(\frac{\partial U_i}{\partial x_j} + \frac{\partial U_j}{\partial x_i}\right)$ is the mean rate-of-strain tensor and

$$\nu_t = c\Delta^2(2S_{ij}S_{ij}) \tag{2.93}$$

with c a constant and Δ a measure of grid resolution. The paper concentrated on a detailed specification of the governing equations and numerical method, although the same model has since been widely used for mesoscale mountain-flow predictions (for example, Smolarkiewicz and Rotunno, 1989,1990). Some preliminary calculations were undertaken for uniformly stratified flow over two-dimensional bell-shaped ridges of low and moderate slopes. In the former case the credibility of the code was established by reference to linear theory. In the second the non-linear treatment of the surface boundary condition (enabled by the surface-fitting coordinate transform) resulted in a highly asymmetric flow field, with large form drag and strong downslope winds on the lee side. These severe downslope winds and non-linear effects on internal-wave propagation have received considerable interest in recent years and we shall return to them later.

Mason and Sykes (1979b) presented time-dependent numerical integrations of the Navier-Stokes equations for a constant-density, uniform-viscosity flow around three-dimensional bell-shaped hills, investigating the response to changes in Reynolds number, aspect ratio and the relative depth of the boundary layer. They drew attention to the difficulty of *defining* three-dimensional separation and related their computed flow patterns to the purely topological constraints set out by Hunt et al. (1978); in particular, to the absence of any closed recirculation zone bounded by a separation surface for three-dimensional obstacles. This has clear implications for dispersion modelling and, in a related paper, Mason and Sykes (1981) demonstrated that the transport of material into a three-dimensional recirculation zone is dominated by advection rather than diffusion. Despite the absence of a turbulence model

(which limits the direct interpretation to real topography), a number of points were made which are worthy of emphasis. Periodic boundary conditions were used in the lateral direction. Besides numerical convenience this has benefits in the calculation of the obstacle-induced perturbation to the viscous drag, which, unlike the pressure drag, would otherwise have contributions from distances far downstream of the obstacle. However, periodic boundary conditions do have some penalties. Although it was shown to have little dynamical role, the Coriolis force has to be included to balance the driving pressure gradient and so obtain a homogeneous boundary layer over level terrain. For time-dependent calculations it was necessary to ensure that the velocity field used as an initial condition satisfied continuity. Mason and Sykes also used a cartesian grid rather than a terrain-following coordinate transformation (Figure 2.6). This required special treatment for the control volumes which straddled the hill surface. However, the authors did point out that the commonly applied criticism that this requires an unnecessarily high density of grid cells over the depth of the hill is somewhat fallacious, since such a concentration of cells would be required anyway to resolve any recirculating flow region.

Examples of the application of computational fluid dynamics to real terrain are comparatively scarce. One obvious reason is the enormous computer resource needed for a complex three-dimensional calculation. A second reason is that experimental data of sufficient detail and quality is not available for a definitive comparison. However, two good examples of finite-volume, real terrain calculations are those of Raithby et al. (1987) for Askervein and Dawson (1991) for Steptoe Butte. The former used a terrain-fitting coordinate mesh whilst the second used a cartesian grid with stair-stepped representation of the topography. Both used the two-equation k-ε turbulence model and both found it appropriate to modify the standard model for atmospheric boundary-layer application, Raithby et al. adopting the revised constant value C_μ=0.033 to conform to observed stress-strain ratios over rough surfaces and Dawson et al. adopting, in addition, Detering and Etling's (1985) revision of the constants in the dissipation equation to include the boundary-layer height. (More will be said about these revisions in Chapter 5).

A common difficulty in comparing with real data is that of specifying the appropriate inflow conditions. Raithby et al. (1987) used a one-dimensional version of the governing equations

with mean velocity fixed at 10m to obtain a definitive inflow profile. For mean-flow profiles they obtained good agreement with experiment on the windward side of the hill and a marked improvement over linear theory in the lee. Shear-stress profiles were far less satisfactory, however, indicating both the deficiencies of the particular turbulence closure and the commonly recognised fact that the *mean* velocity field is often comparatively insensitive to the details of the turbulence model. Given the coarseness of the grid (20×20×19 nodes) and the highly diffusive upwind differencing scheme used, it is probable that the flux terms were dominated by numerical diffusion.

Dawson et al. (1991) used their PEST code to simulate dispersion from upwind sources in the Steptoe Butte dispersion experiment. Key aspects of this experiment were the ambient stability and the presence of an extensive three-dimensional separation in the lee, into which a considerable amount of material was advected. An interesting feature of their dispersion simulation was the testing of a "gaussian-initialisation" procedure to replace near-source concentrations with analytically-defined values, rather than applying the numerical model directly with the source strength smeared uniformly across one grid cell. They found the modification to make little difference to ground-level concentrations. A comparable technique has been used in our own code SWIFT (see Chapter 3) - with comparable results.

Wood and Mason (1993) used a one-equation (k) eddy-viscosity model to examine the pressure drag induced by neutrally stable boundary-layer flow over three-dimensional hills. They concluded that the perturbation to the net surface force imposed by the obstacle was dominated by the pressure drag, which was, however, very sensitive to the turbulence closure used. In conjunction with a second-order linear analysis they established the validity of an "effective-roughness-length" parameterisation of the surface drag due to topography smaller than the grid scale in numerical weather-forecasting models.

Strongly Stratified Flow

Hitherto, we have considered computational models of boundary-layer flow over hills in which the turbulence model is significant but in which buoyancy forces play a comparatively

subordinate role. We turn our attention now to flows around topography where buoyancy effects are dominant. Particular areas of interest in this respect are the intermediate Froude number range (Fr=O(1)) for which no analytical theory exists, the prediction of non-linear internal gravity waves (and in particular, the association of breaking waves with highly asymmetric flows, high-drag states and severe downslope windstorms) and the prediction of slope winds caused by surface cooling.

Smolarkiewicz and Rotunno (1989,1990) carried out an important series of computations of uniformly stratified flow around three-dimensional bell-shaped topography using Clark's (1977) non-hydrostatic model with a grid-nesting procedure (allowing simultaneous solution on a sequence of grids of differing spatial resolution). Their parameter range bridged the gap between the high-Froude-number regime, where linear theory is applicable, and very-low-Froude-number flow (Drazin, 1961), where the strong stratification forces effectively horizontal potential flow around the hill contours. Their calculations successfully reproduced the predictions of both theories at the limits of the Froude-number range and demonstrated that linear theory could give qualitatively good predictions far below the Froude numbers for which it is formally valid. Indeed, Smith's (1980) linear theory of hydrostatic flow over a hump was shown to give a good prediction of the location of, and critical Froude number for, upstream stagnation, despite violating the fundamental assumption of small-amplitude perturbations. As the Froude number ($Fr=U/NH$) was reduced below 0.5 the computations revealed the development of two important flow features (Figure 2.7): a pair of vertically-oriented lee vortices and an upwind flow-reversal zone. Since Smolarkiewicz and Rotunno used a "free-slip"/stress-free lower boundary condition, these could not be ascribed to the usual viscous phenomena of boundary-layer separation or "horseshoe-vortex" roll-up and could, therefore, be generated (in density-stratified flows) by purely inviscid processes. (It is an advantage of numerical tools that, by eliminating certain obscuring features such as viscosity or rotation, it becomes possible to identify *mechanisms* for various flow features. In the laboratory, of course, viscous and inviscid phenomena exist side by side and it is not always possible to separate the two.) Smolarkiewicz and Rotunno demonstrated that (horizontal) vorticity could be generated baroclinically via the density-gradient term in the vorticity equation:

$$\frac{\nabla\rho\wedge\vec{g}}{\rho} \tag{2.94}$$

and, by application of a linear theory (expanded to second order), that the vortex lines could be advected and rotated to form the vertically-oriented vortex doublet in the lee of the hill. In their 1990 paper Smolarkiewicz and Rotunno showed that the initial upwind stagnation which caused the roll-up on the front face could be caused by two distinct effects: the hydrostatic pressure built up by the density perturbation aloft associated with the standing mountain wave (essentially Smith's (1980) mechanism) or the upstream propagation of columnar modes admitted by the reflecting layer caused by lee-wave breaking. By conducting a series of tests for different aspect ratios they concluded that the former effect was dominant for axisymmetric hills and that the latter effect became more significant as the relative width of the hill increased, approaching the two-dimensional limit.

Three-dimensional stratified flow calculations over a similar range of Froude numbers have been carried out by Miranda and James (1992) in the context of topographic drag. They adopted the meteorological practice of using pressure- rather than height-based vertical coordinates, which has some advantages in the formulation of the thermodynamic equations in atmospheric flows. The authors drew attention to the dangers implicit in using drag parameterisations based on two-dimensional flow phenomena - especially the high-drag, severe-downslope-windstorm state (see below) - which do not take into account the extra degrees of freedom permitted by three-dimensional disturbances. Their computations indicated three Froude-number regimes: $Fr>2$, where the disturbance was qualitatively well-described by linear theory; $Fr<0.5$, where the flow is characterised by horizontal streamline splitting and the upwind-flow-reversal/downwind-vortex-pair features already described by Smolarkiewicz and Rotunno (1989,1990); and an intermediate region characterised by wave breaking and periodic variations in surface wave drag.

The interaction between buoyancy forces and topography extends beyond the stability profile of the approach flow. In light winds downslope (katabatic) or upslope (anabatic) winds are driven respectively by cooling or heating of slopes. According to Defant's (1951) description of local winds, nocturnal sidewall cooling of valleys leads to a downslope flow with a pooling

of heavy air at the centre of the valley. MacNider and Pielke (1984) describe a three-dimensional, hydrostatic, primitive-equation model forced by a surface-energy budget. Their simulations (in both idealised and real-terrain configurations) are broadly in line with this description and reveal a very shallow sidewall slope flow developing quickly, with a much deeper secondary down-valley flow lagging about an hour behind. A comparatively simple turbulence model was used with eddy-transfer coefficients dependent on the local gradient Richardson number. The simulations also reveal regions of high turbulence intensity at the top of the slope flows where the downslope advection caused local overturning of the potential-temperature isentropes and, consequently, an unstable density gradient. Drainage flows were also simulated by Heilman and Takle (1991) using a more advanced turbulence closure (Mellor-Yamada level 3 - broadly equivalent to an algebraic stress model).

For strongly stratified flow the hydrostatic approximation - which neglects the vertical acceleration and computes the pressure distribution directly by integration of the density profile, so bypassing the need to solve a Poisson equation for pressure - is widely used. However, a number of non-hydrostatic effects can be of great significance. For example, neglect of the vertical acceleration means that hydrostatic models cannot be used to compute flow recirculation zones. In linear theory the hydrostatic approximation implies that all modes may propagate, whereas, in practice, sufficiently short waves are evanescent. If the stability weakens (or wind speed increases) aloft then waves which propagate in the lower layers may not be able to do so in the upper layer and will be reflected. Thus, lee-wave trapping is an essentially non-hydrostatic phenomenon. Yang (1993), using a one-equation turbulence closure with a terrain-following coordinate system and contravariant velocity decomposition, showed that this continues to hold true in the non-linear regime. Yang also commented that the hydrostatic approximation tends to exaggerate the pressure gradient due to differential surface heating so that, for example, hydrostatic sea-breeze systems are over-developed. The general implications of the hydrostatic approximation for realistic atmospheric wind speed and potential temperature profiles have been analysed by Keller (1994).

Concluding Remarks

This brief review of the literature has followed the development of numerical modelling of flow over topography from the early 1970s to the present day. In that time we can identify a steady progress from two-dimensional calculations with simplified flow equations to a full three-dimensional capability. At the same time, increasing computer power has enabled us to study the effects of the turbulent and thermal structure of atmospheric boundary-layer flow over topography.

Although many of the numerical models are applicable, in principle, to arbitrary terrain the emphasis to date has been on idealised hill shapes and what real topography has been studied has been, at best, under-resolved. The linkage of dispersion predictions with flow calculations has also been little pursued. Our own calculations of flow around Cinder Cone Butte - to be presented in Chapter 6 - will go some way to remedying these deficiencies.

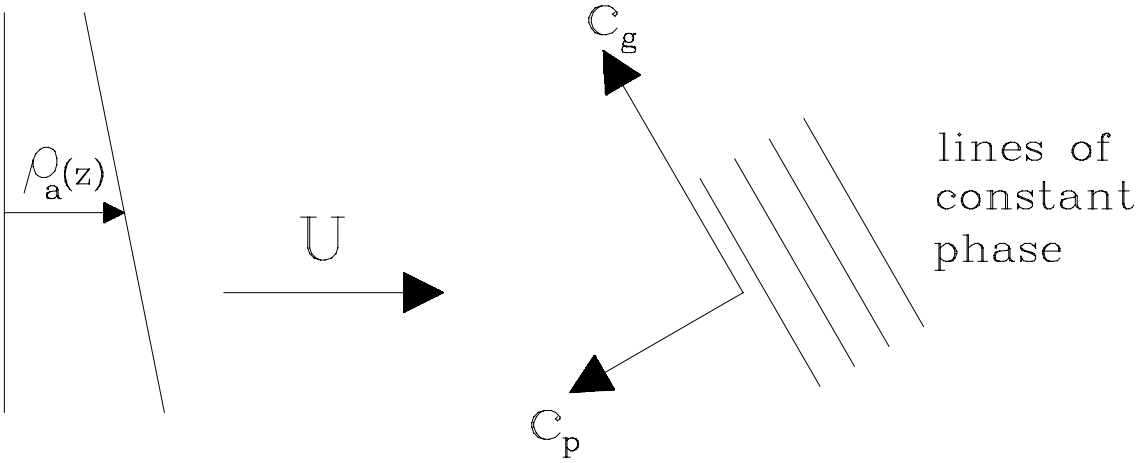

Figure 2.1: Direction of phase and group velocity (relative to mean wind) for outgoing, topographically-generated internal gravity waves.

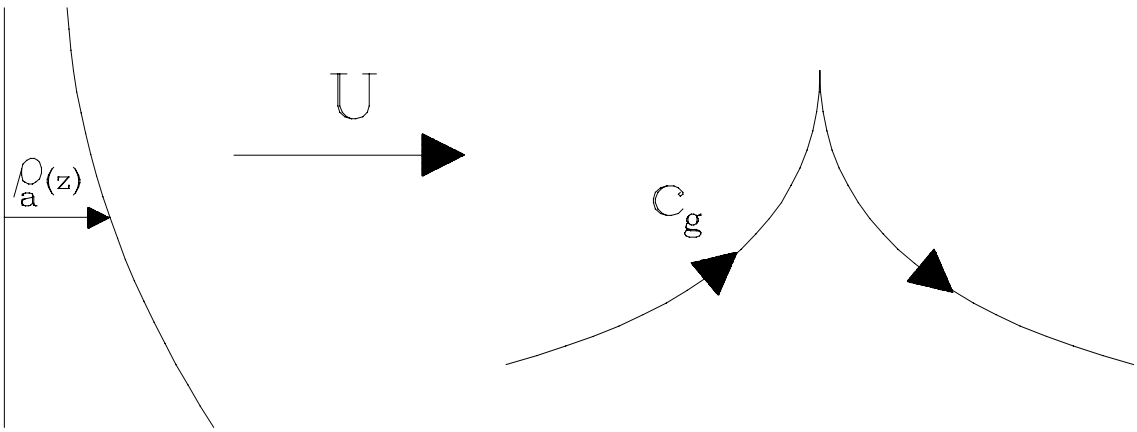

Figure 2.2: Cusped path of reflected waves in a weakening density gradient.

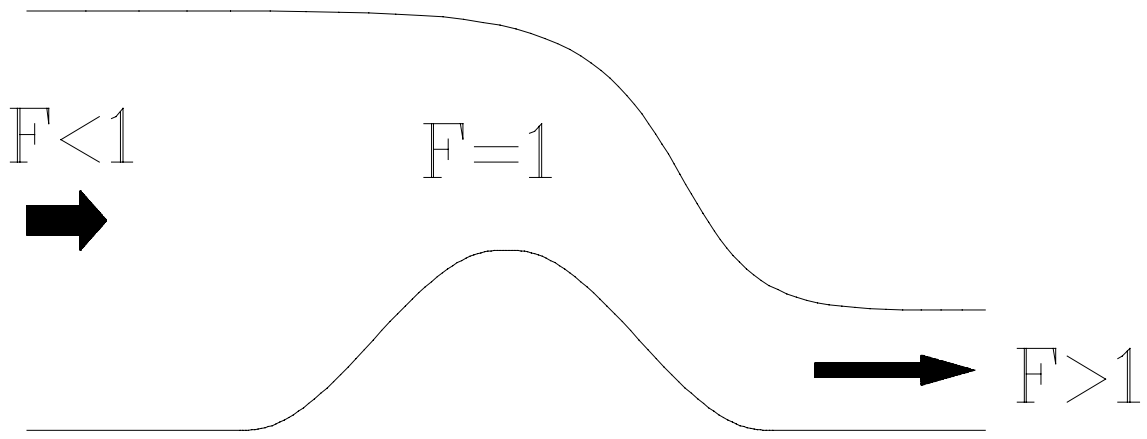

Figure 2.3: One-layer hydraulic transition.

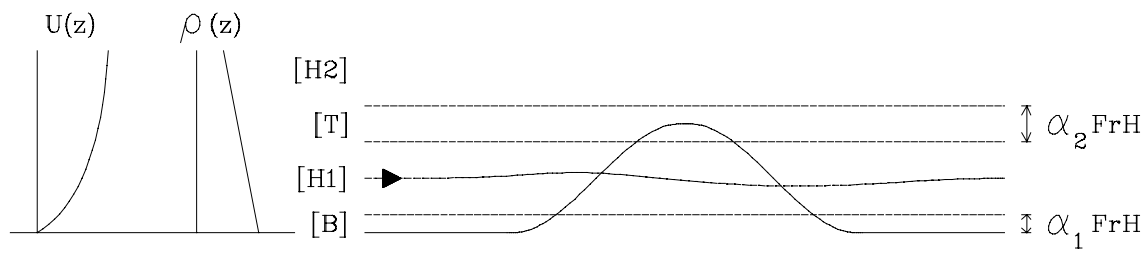

Figure 2.4: Drazin's model.

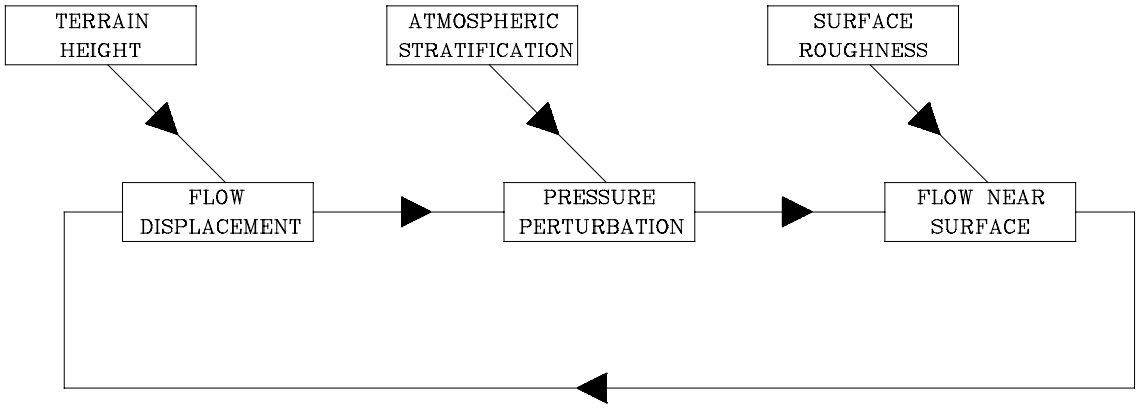

Figure 2.5: Development of the flow perturbation over topography.

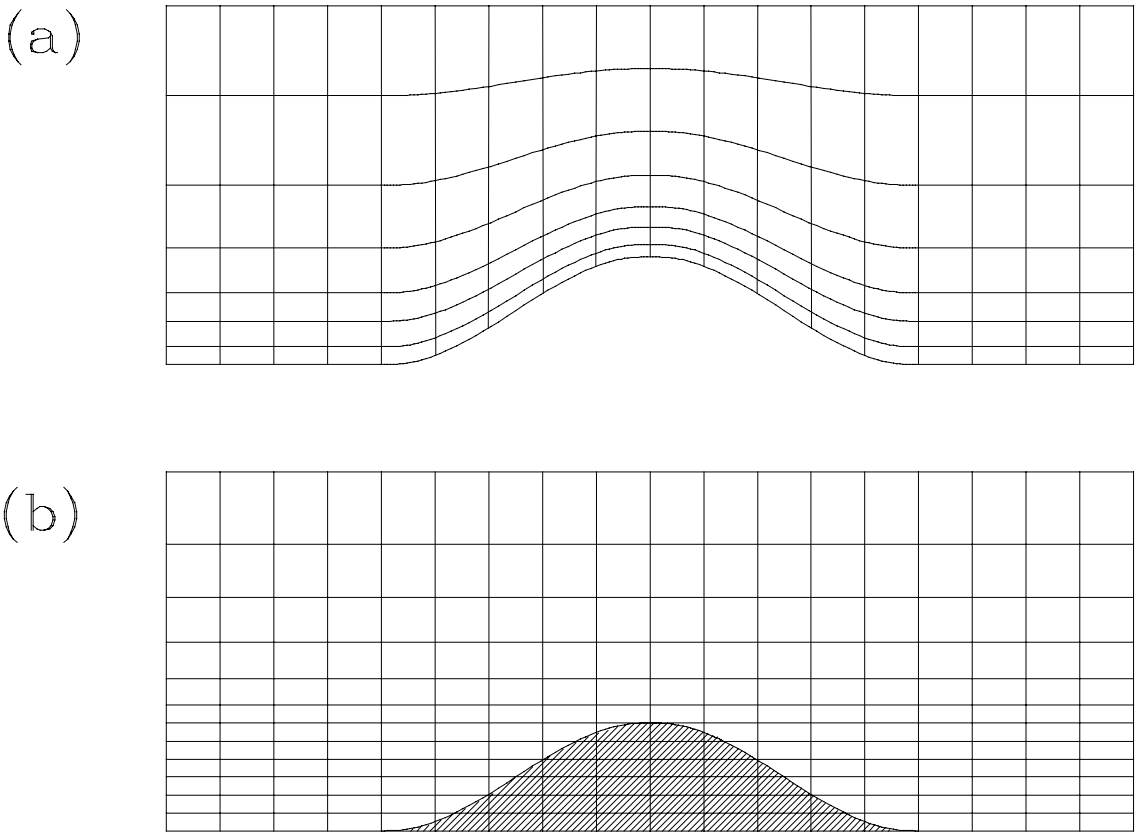

Figure 2.6: Mesh types for computation of flow over hills; (a) terrain-following; (b) cartesian.

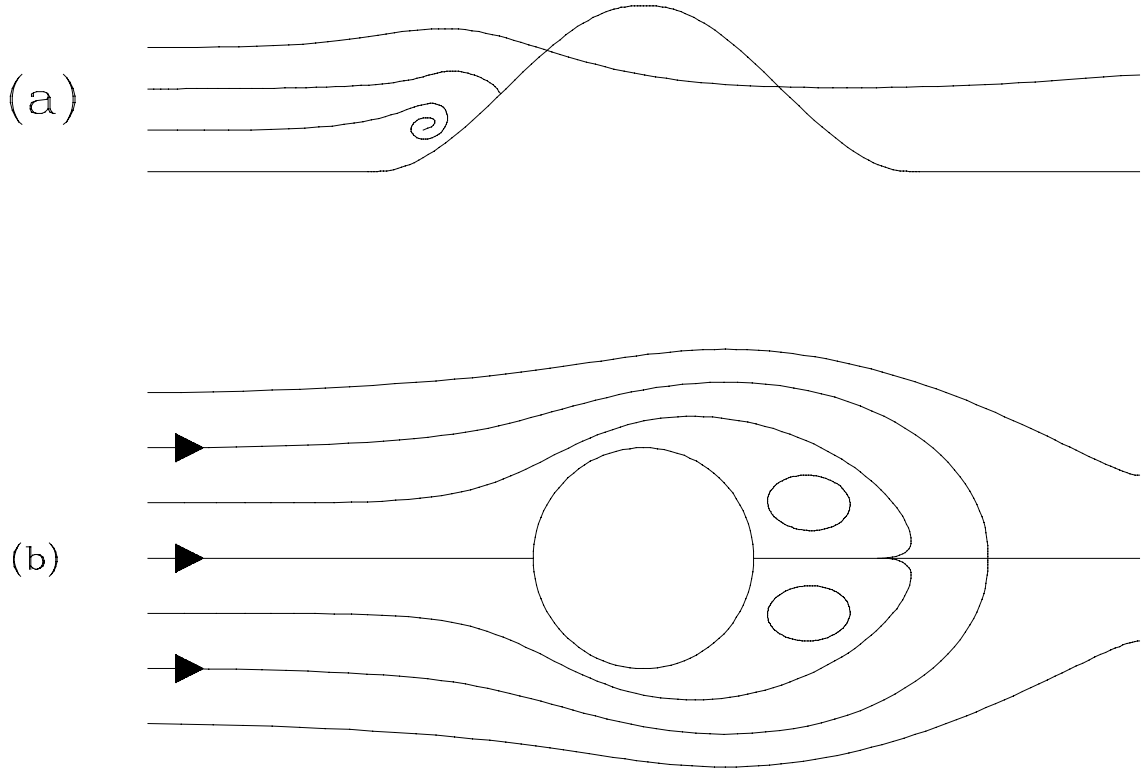

Figure 2.7: Vortex structures in inviscid, stably stratified flow around an axisymmetric hill; (a) upwind flow reversal; (b) baroclinically-generated lee vortices.